



LEBANESE UNIVERSITY
FACULTY OF ENGINEERING
UNIVERSITY INSTITUTE OF TECHNOLOGY

Master 2 Specialized Project Report

Civil Engineering – Option Petroleum Structures (Ch. E)

2017-2018

**Photocatalytic degradation of
microplastics by ZnO nanorods**

Bouthayna Alrifai

Presented in
Jury:

13/09/2018

in front of the

Dr. Wael Hamad

Supervisor

Dr. Nelly HOBEIKA

Reviewer

Dr. Rafic YOUNES

Examiner

Work performed at the Laboratory Functional Materials
and supervised by:

Prof. Joydeep Dutta

Dr. Wael Hamad

Acknowledgement

I would like to express my deep gratitude to all those who have helped me, from near or far, to carry out this project.

I sincerely thank KTH University, Applied physics department for giving me the chance to complete my thesis, especially the Prof. Joydeep Dutta and all the laboratory team who have guided me throughout the realization of this project. They have always been available, listening to my questions, and always interested in the progress of my work. Also I would like to thank the Dr. Wael Hamad from the Lebanese university, faculty of engineering for his understanding, wisdom, and patience.

My thanks also go to the faculty and administrative department in the faculty of engineering of the Lebanese University for the great efforts they make to ensure that their students having a good training and the maximum of needed information.

Abstract

In this project we were interested in studying the problem of water pollution: causes, effects on human being lives and the ecosystem, and existing techniques used to reduce its rate while citing the advantages and disadvantages of each of them.

This project focused on the use of the photocatalysis process to photodegrade microplastic pollutants by semiconductor photocatalysts into harmless end products such as carbon dioxide and water. Here we report the fabrication of visible light active zinc oxide nanorods (ZnO NRs) using the hydrothermal method, in which Methylene Blue (MB) had been used as an organic model to study the different photodegradation aspects. Wherein, the main goal was to study the effect of doping these NRs by N-doped graphene quantum dots-Urea on the absorbance and photoluminescence spectrum of ZnO NRs and on the photodegradation rate of MB.

Keywords: water pollution, photocatalysis, nanoparticles, semiconductor, microplastics, zinc oxide, graphene, band gap, electron-hole pairs, conduction band, valence band.

Résumé

Ce travail a été effectué pour mettre en évidence le problème de pollution de l'eau: ces causes, ces effets sur les autres vivants et les solutions existantes pour réduire le taux tout en citant les avantages et les inconvénients de chacun d'eux. Ce projet s'est intéressé surtout sur l'utilisation du processus de photocatalyse pour photodégrader les polluants microplastiques par des photocatalyseurs à semiconducteurs. Le but principal était d'étudier l'effet de l'imbrication de ces NRs par le graphène quantique-urée à points dopés N sur le spectre d'absorbance et de photoluminescence des ZnO NRs et sur le taux de photodégradation du MB.

Mots clés: photocatalyse, nanoparticule, semiconducteur, microplastique, oxide de zinc, graphène, paires electron-holes, bande de conduction, bande de valence.

Table of contents

Introduction.....	11
Chapter 1: Plastic pollution	13
1.1.Sources of microplastics.....	13
1.2. Effect of plastics and microplastics	15
1.3. Minimizing water pollution.....	16
Chapter 2: Photocatalysis.....	17
2.1. Metals, Semiconductors and insulators.....	17
2.2. Semiconducting material.....	18
2.3. Application.....	18
2.3.1. Removing trace metals.....	18
2.3.2. Antibacterial and cancer treatment.....	18
2.3.3. Self-sterilization.....	19
2.3.4. Water splitting.....	19
2.3.5. Water treatment.....	20
2.3.5.1. Photocatalytic materials.....	20
2.3.5.2. Mechanism.....	21
Chapter 3: Synthesis of zinc oxide nanorods.....	24
3.1.Classification of ZnO and choice of the structure.....	24
3.2. Synthesis techniques of Zinc oxide nanomaterials.....	26
3.2.1. Nanorods growing procedure.....	27
3.2.2. Effect of growing parameters on the photocatalytic activity.....	28
3.3. ZnO properties affecting the photocatalytic process.....	31
3.4. Improvement of ZnO as photocatalyst.....	33
3.4.1. Metal/non-metal doping.....	33
3.4.2. Depositing of noble metals.....	34
3.4.3. ZnO coupling with other semiconductors.....	34
3.4.4. Coupling of nanocarbon component to ZnO.....	35
3.4.5. Crystal growth and shape control.....	36
3.4.6. Surface modification of ZnO.....	37
Chapter 4: Methodolgy.....	38
4.1.Preparation of ZnO nanorods coated glass substrates.....	38
4.1.1. Materials.....	38
4.1.2. Procedure.....	38
4.2. Preparation of SnO ₂ /ZnO NRs composite.....	38
4.2.1. Materials.....	38
4.2.2. Procedure.....	38

4.3. Synthesis of N-doped Graphene Quantum Dots-Urea.....	39
4.3.1. Materials.....	39
4.3.2. Procedure.....	39
4.4. Deposition of N- doped graphene quantum dots-Urea on ZnO NRs and on SnO ₂ /ZnO NRs composite surface.....	39
4.5. Characterization.....	40
4.6. Results and discussion.....	40
Conclusion.....	49
References.....	50

List of figures

Figure 1- (a) Causes of water pollution (b) ratio of plastics to fish in the ocean (c) sources of microplastics.....	14
Figure 2- Effects of water pollution on animals and human being lives.....	15
Figure 3- Schematic diagram showing a comparison of the energy band gap for insulators, semiconductors, and metals.....	18
Figure 4- Photocatalytic water splitting	19
Figure 5-Band positions of some semiconducting materials.....	21
Figure 6- Figure 6: Mechanism of the photocatalytic reaction.....	23
Figure 7- FESEM and SEM images for (a) 0D, (b) 1D, (c) 2D, (d) 3D zinc oxides.....	25
Figure 8- Photocatalytic degradation of methylene blue using ZnO nanoparticles and nanorods on glass substrates upon excitation with light from a tungsten halogen lamp (~72 klux).....	25
Figure 9- Normalized concentration against irradiation time when 5 μ M aqueous.....	29
Figure 10-variation in the visible emission peak from the ZnO NRs annealed at different temperatures.....	29
Figure 11-Photocatalytic degradation profile of 10 mM methylene blue (MB) in aqueous solution under visible light irradiation with ZnO NRs photocatalysts annealed at different temperatures (90, 150, 250, 350 and 450 °C for 1 h). (a) Degradation kinetics of MB; (b) degradation rate constants of MB.....	30
Figure 12-Schematic representation for the mechanism of antibacterial activity of ZnO NRs.....	32
Figure 13-SEM micrographs: (a); (b) and (c) top views; (d); (e) and (f) cross-sectional views of ZnO nanorod arrays grown hydrothermally for 15 h, using precursor concentrations of 2 mM, 10 mM and 40 mM, respectively.....	33
Figure 14-Schematic of the comparison of the band structures of pure, metal-doped ZnO, and nonmetal-doped ZnO.....	35
Figure 15-Photogenerated charge separation mechanism of ZnO coupled with $\text{TiO}_{2-x}\text{N}_y$	35
Figure 16-Schematic transfer process of GQDs coated ZNRA.....	36
Figure 17-Effect of OH^- concentration towards the mechanisms of ZnO formation.....	39
Figure 18-(a) Substrates cleaning process in VWR ultrasonic cleaner (b) Seeding the substrates using the spray pyrolysis method (c) Chemical bath of the seeded substrates (d) Annealing of the substrates in an atmospheric furnace at 350°C.....	40
Figure 19-(a) N-doped GQDs- U solution (b) ZnO NRs /N-doped GQDs-U substrate.....	41
Figure 20: SEM micrographs of ZnO nanorods.....	42
Figure 21-Deconvoluted PL spectra of ZnO NRs for an excitation wavelength $\lambda_{\text{Ex}} = 320$ nm.....	43
Figure 22- (a) UV-vis spectrum of the N-doped GQDs-U suspension (b) tauc plot of the absorption curve of N-GQDs-U (c) Photoluminescence spectra of N-doped GQDs-U.....	45
Figure 23-(a) UV-vis absorption spectra of the ZnO NRs and N-GQDs-U/ZnO NRs (b) PL spectra of ZnO NRs and N-doped GQDs-U/ ZnO NRs for an excitation wavelength $\lambda_{\text{Ex}} = 320$ nm.....	46
Figure 24-PL spectra of the Synthesized ZnO NRs, SnO_2/ZnO NRs composite and N-GQDs-U/ SnO_2/ZnO NRs composite.....	46
Figure 24-Time variation of photocatalytic activities of ZnO NRS, N-GQDs-U/ZnO NRs, SnO_2/ZnO NRs composite and N-GQDs-U/ SnO_2/ZnO NRs composite under (a) UV light conditions (b) visible light conditions.....	49

List of tables

Table 4.1- Advantages and disadvantages of different ZnO nanostructures used in photocatalytic applications.....	23
--	----

List of symbols

AOP: Advanced Oxidation process

CB: Conduction band

CV: Valence Band

MB: Methylene blue

NPs: Nanoparticles

NRs: Nanorods

ZnO: Zinc Oxide

SnOx: Tin Oxide

Eg: Band gap

UV: Ultraviolet

GQD: Graphene quantum dots

h ν : Photonic energy electrons

e⁻: Electron

h⁺: Hole

Introduction

Water pollution is the finest topic to discuss in the modern era and it has become the most popular concern in recent years. With industrial development, environment pollution yields high amounts of organic contaminants, and this is a serious problem [1, 2]. In addition, microplastics in aquatic ecosystems and especially in the marine environment represent a pollution of increasing scientific and societal concern. Since the middle of the 20th century, the increasing global production of plastics is accompanied by an accumulation of plastic litter in the marine environment. Various biological, chemical and physical techniques have been used for the treatment of water system [3]. The main drawback of these techniques is formation of secondary waste product. Thus, attention has been focused on the oxidation of organic compounds to harmless products using the oxidation advanced process (AOP) and especially on the photocatalysis process to remove organic contaminants and noxious bacteria using the solar power and semiconductor-based photocatalysts [4-6]. The efficiency of the semiconductor photocatalysts, such as ZnO [7, 8], TiO₂ [9-13], CdS [14, 15], ZnS [16], SrTiO₃ [17, 18], C₃N₄ [19-22], and BiOI [23, 24], is generally determined by light absorption, in which electrons are excited from the valence band to the conduction band, leaving a hole (h^+) in the valence band, and immediately exciting photoredox reactions.

Zinc oxide semiconductor is an important photocatalyst. Thereby it has been widely examined because of its excellent properties over the other photocatalysts such as TiO₂, including low price, high redox potential, nontoxicity, and environmentally friendly features [25-29]. Plus, ZnO yields a wide band gap (3.37 eV) and a high excitation energy (60 meV) [30]. Thus, it can absorb a larger fraction of the ultraviolet (UV) spectrum and exhibit a greater photocatalytic performance than TiO₂ in the photodegradation of organic contaminants [31-35]. It is a promising antibacterial agent because of its good thermal stability, high antimicrobial activity, and excellent biocompatibility [36-39]. ZnO NPs are also non-toxic and biocompatible with human cells [40-42]. However, this big band gap allows the ZnO photocatalyst to absorb only UV light, which constitute only 4% of the solar spectrum, but not the visible light, which constitute 43% of the solar spectrum [43]. In addition, the fast recombination of the photogenerated electron-hole pairs diminishes the performance of ZnO photocatalysts. Thereby, modifications in ZnO have been made in order to extend its visible-light response and reduce the rate of recombination of electron-hole pairs [44, 45] using different methods, such as metals/non-metals doping [46-49], noble metals deposition [50-53], constructing heterojunctions [54-58], and coupling carbon materials [59-64]. Noble metals such as Pt, Au and Ag are usually used with ZnO to form hybrid nanostructure, which leads to improved photocurrent and ultraviolet photoresponse. Quantum dots have widely used to decorate ZnO for enhancing the photocatalytic activity. The decorating of QDs on ZnO nanostructures can generate a new interface and enhance charge separation; thereby efficient transfer from QDs to the conduction band of ZnO takes place, which can improve the photoresponse under ultraviolet light irradiation. However, considering the high price, limited mineral sources of noble metals, and toxicity of QDs, searching for a low-cost and eco-friendly new materials to replace these nanomaterials and thus to improve the performance of ZnO nanomaterials is urgent and important. Recently, graphene quantum dots GQDs, single- or few layer graphene with a tiny size of only several nanometers, are attracting more and more attention because they are nontoxic, biocompatible, cheaper and they exhibit other advantages such as their higher penetrability into pores and small spaces because of their remarkably smaller size, their high semiconducting properties and their many more active edged. Thus, this project aim to show the preparation of N-doped GQDs-U/ZnO NRs, and to report the effect of doping the ZnO NRs, synthesized via hydrothermal method, by these GQDs on the absorbance and photoluminescence spectrum of these NRs and on the photodegradation rate of MB.

In addition, this project reports the preparation of SnO_2/ZnO NRs composite, mainly used to protect the NRs from the photocorrosion, and the influence of the Tin oxide on the activity of ZnO NRs as photocatalyst.

Chapter 1: Plastic pollution

Nowadays, wide applications of plastics result in plastic waste being present in the water environment in a wide variety of sizes. Since the development of the first plastic “Bakelite” in 1907, a number of cheap production techniques have been developed to mass produce the modern day plastics. Plastics started to enter the ocean in increasing quantities from the 1950s from a wide variety of land and sea based sources; river, run-off, beach-goers and tourists, ship. Plastic wastes are in water mainly as microplastics (the size range of 1 nm to < 5 mm). Microplastics have been recognized as an emerging threat, as well as ecotoxicological and ecological risk for water ecosystems. The most visible and disturbing impact of microplastics are their ingestion and consequent suffocation of hundreds of marine species. Microplastics can contribute considerably to the transport of non-indigenous marine species to a new area thereby threatening the marine biodiversity and the food web. Therefore, assessment of the status, effect and mitigations are needed.

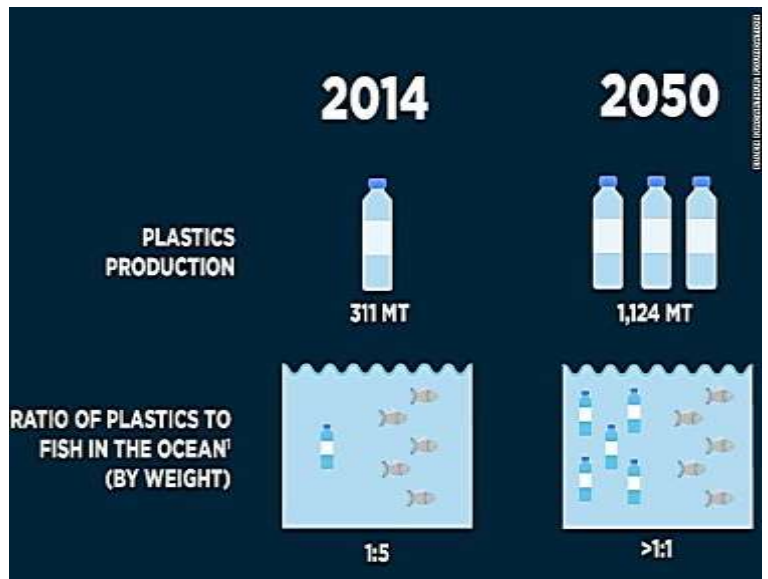
1.1. Sources of microplastics

Synthetic polymers, commonly known as plastics, are the most common pollutants threatening the water system since it plays an important role in the men everyday lives, it is essential for the economy and can be found in a large variety of consumer products in which are designed to be discarded within three years of their production [65, 66]. Conventional materials such as metal, glass, and paper have being replaced by plastic packaging due to their low cost, excellent oxygen/moisture barrier properties, bio-inertness and their light weight. The annual global demand for plastics has therefore consistently increased and presently stands at about 245 million tons [67, 68]. Nearly a third of the plastic resins production is therefore converted into plastic packaging materials that include disposable single use items. There are a wide range of plastics classes being used in packaging, such as: Polyethyelene (PE), Polystyrene (PS), Polypropylene (PP), Polyethylene terephthalate (PET), polyurethane (PU) and Polyvinyl chloride (PVC) [71]. A wide variety of chemical additives are incorporated into plastic polymers to add particular properties, for example bisphenol A and phthalates [72, 73]. Some additives are designed to stabilize the polymer and make it more resistant towards degradation. The additives are not covalently bonded to the polymer, so they can leach out of the plastics as they degrade and enter into the marine environment [74].

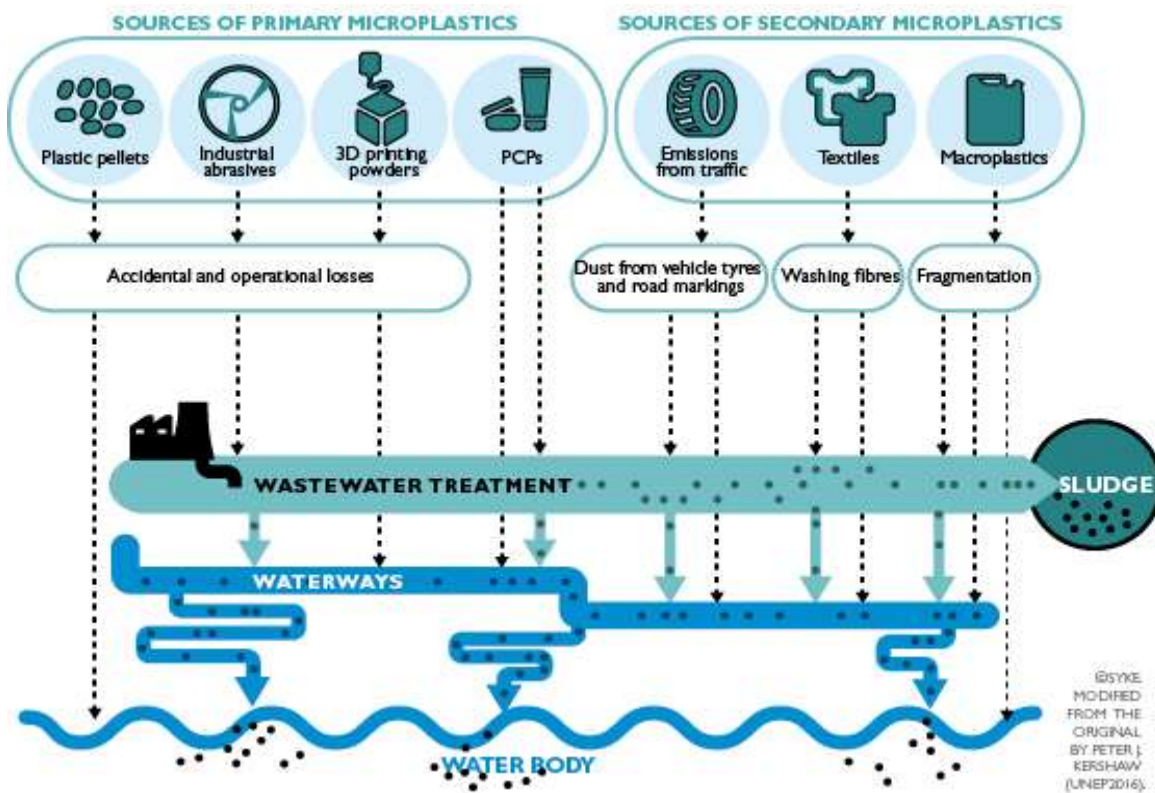
More recently, the discovery of microplastics has raised among scientists, the microplastics are defined as plastic pieces with less than 5 mm in diameter so they are not readily visible to the naked eye so they can't be removed easily from the environment (see figure 1c). There are two classifications of microplastics: primary and secondary microplastics. Primary microplastics are manufactured and are direct result of human material and product use such as cosmetics and personal care products. Secondary microplastics enter the environment through fragmentation and degradation of larger plastic items from exposure to the sunlight, freezing, wind, wave action, and abrasion. Another important source of secondary pollution by microplastics occurs from the breakdown of synthetic fibers and discharge into the environment through waste water from washing machines [69, 70].



(a)



(b)



(c)

Figure 1: (a) Causes of water pollution (b) ratio of plastics to fish in the ocean (c) sources of microplastics [253].

1.2. Effect of plastics and microplastics

Water pollution has many negative effects on humans and also on the environment [75-78]. The existence of pollutants in water can cause serious damage to the fish lives since they can raise the temperature of the water to a level that may force the fishes out in search of cooler waters, and this in turn can create an ecological dead zone. In regard to plant life, pollution can increase the rate of algal blooms, which in turn causes the fish and other gill-bearing animals to suffocate as the oxygen in the water gets is depleted. In addition, ingestion of plastics by birds and turtles is a major problem and it is extensively documented worldwide, where at least 44% of marine bird species are known to ingest plastics [80]. In addition, and due to the small size and persistence of microplastics, they have been found throughout our environment. They have been found in all forms of our life; in table salt, sugar, honey, and beer; in organic fertilizers; in the dust in our homes; and also in bottled and tap water samples [79]. They have been found in the tissues of fish and shellfish species that are sold in stores and markets. Besides to the sicknesses and diseases that affect the fish, marine birds and the other oceanic animals and even the humans, a major danger and a serious problem are looming and threatening all living organisms known as "congenital malformations".

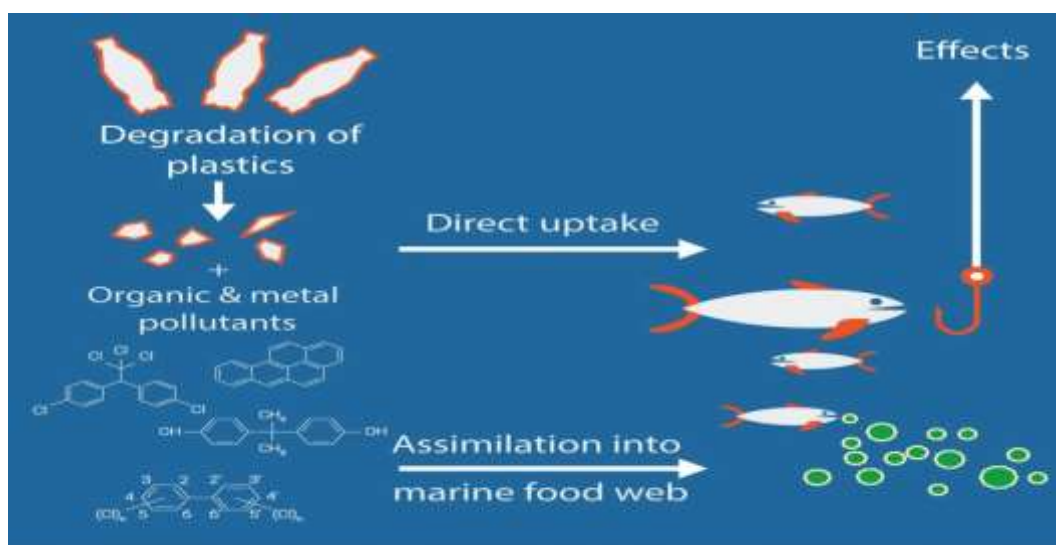


Figure2 : Effects of water pollution on animals and human being lives [254].

1.3. Minimizing water pollution

The last decades have shown a reevaluation of the environmental pollution issue, both at regional and at international level. Reducing the amount of pollutants in water remains the main goal of the most of nations in order to reduce the diseases caused by water pollution. Stop throwing the plastic garbage away, buy environment-safe cleaning products, reduce the amount of insecticides and pesticides used in agriculture and reduce the waste of water are the main ideas that came to the mind to minimize the water pollution. However, since wastewater from industries and sewage are the main sources that affect and can significantly increase the rate of water pollution, and since the microplastics are not readily visible to the naked eye, the development of effective and affordable technologies to treat these pollutants is therefore the effective way to reduce the rate of pollution.

In the past, several physical techniques like coagulation, flocculation, sand filtration, adsorption on the activated carbon, and chemical methods like photosensitized oxidation, adsorption [81-84], have been used to reduce the toxic effluents from waste water [85-88]. However, the main drawback of these techniques is formation of secondary waste product which cannot be treated again and dumped as such [89, 90]. Therefore, attention has been focused on the oxidation of organic compounds to harmless products such as CO_2 and H_2O using the advanced oxidation process (AOP) which is developed in the 1970s, and is suitable for the oxidation of a wide range of organic compounds. AOPs can be classified into two groups; the non-photochemical AOPs that include ozonation, wet air oxidation, etc., and the photochemical AOPs that include homogeneous processes (UV/ozone/hydrogen peroxide, UV/hydrogen peroxide, etc.,) and heterogeneous processes (photocatalysis process, which is the very advanced oxidation processes (AOP) and it is used for the photodegradation of toxic compounds and for the purification of water).

AOPs have gained popularity during the past two decades for the treatment of industrial effluents because of their many advantages [91, 92] over the traditional methods such as:

- They have high degradation efficiency.
- They have potency against a wide array of pollutants to reduce the toxicity and completely mineralize organic contaminants.
- The production of hazardous by products into water bodies is negligible.
- They do not produce sludge as in the case of physical, chemical, or biological processes.
- They have nonselective pathway which allows the treatment of different organic pollutants.
- They are cost effective.

Chapter 2: Photocatalysis

“Photocatalysis” is a Greek word, which is a combination of two words: photo that came from “phos” which means light, and catalysis that came from “katalyo” which means break apart or decompose. Photocatalysis is an accelerated photochemical process by the presence of a catalyst and it is based on the activation of a photocatalyst by the action of irradiation with an appropriate wavelength. It is known as the very advanced oxidation process, and basically, it is divided into two categories: homogenous photocatalysis (when the reactants exist in the same phase) and heterogeneous photocatalysis (when the reactants exist in different phases). It is a good replacement for the energy-intensive conventional treatment methods because of using renewable and pollution-free solar energy, this process produces harmless products, unlike conventional treatment measures which transfer pollutants from one phase to another, it can be used in the destruction of a wide variety of hazardous compounds in different wastewater streams, in addition, the reaction conditions for photocatalysis are mild, a lesser chemical input is required and the reaction time is modest.

2.1. Metals, Semiconductors and insulators

When two atoms are brought together to form a molecule, their atomic orbitals are shared to yield bonding and antibonding molecular orbitals. Valence electrons occupy the new orbitals in a way that only bonding orbitals are filled. If the number of atoms constituting the molecule increases, the number of molecular orbitals will grow progressively. If the amount of atoms implied in bonding approaches the Avogadro's number, as it occurs in conventional solids, the energy levels of the electrons contributing to bonding will develop a virtual continuum of energy levels known as valence band (VB). In the same way, the more energetic antibonding orbitals will merge to form a continuous band of unoccupied states called conduction band (CB). So, there are two possibilities, either the occupied or the unoccupied states will merge together in more electronic levels than bonding electrons, or a void band with no available energy states will develop between the occupied and unoccupied levels. The first situation corresponds to metallic bonding, which is relatively weak and not directional interactions between atoms of the same kinds, and the other type corresponds to either semiconductor or insulating solids, depending on the magnitude of the forbidden band. So for the insulating solids, the energy gap between the highest filled levels and the lowest empty levels is so large that the empty levels are inaccessible: thermal energy cannot excite an electron from a filled level to an empty one. And for the semiconductors, the difference in energy between the highest occupied level and the lowest empty level is intermediate between those of metals and insulators (see figure 3).

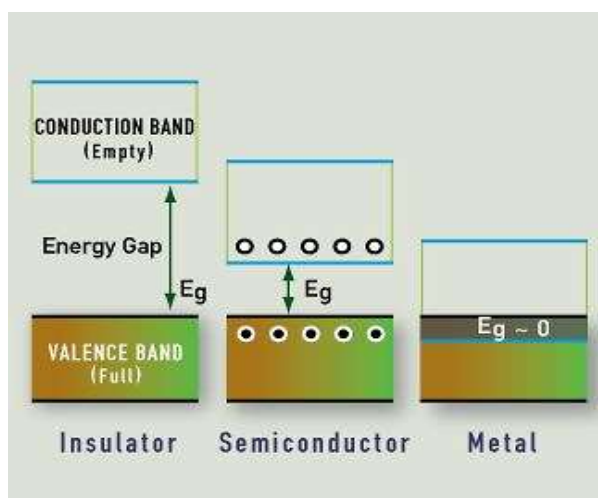


Figure 3: Schematic diagram showing a comparison of the energy band gap for insulators, semiconductors, and metals [255].

2.2. Semiconducting materials

Semiconductors are classified into binary, ternary and quaternary categories. Binary semiconductors include ZnO, TiO₂, Al₂O₃, SnO₂, ZrO₂, CdS, ZnS etc.,. Ternary semiconductors include SrZrO₃, PbCrO₄, Cu₂SnS₃ and so on [93- 95], and quaternary oxides and sulfides include FeZn₂Cu₃O_{6.5}, Bi₂AlVO₇, Cu₂ZnSnS₄ and so on [96- 98].

2.3. Application

The photocatalysts are used in the water and air purification, self-cleaning, self-sterilization, antifogging, antimicrobial activity, and so on. They also can be used for damaging microorganisms, such as bacteria and viruses, and even in activating some cancer cells, as well as for the photosplitting of water to produce hydrogen gas which is the fuel of the future.

2.3.1. Removing trace metals

Some elements such as plumb, chrome, mercury and other metals are extremely hazardous to human health. These toxic metals can be successfully removed, even at lower concentration, by heterogeneous photocatalysis to maintain the water quality and therefore the human health.

2.3.2. Antibacterial and cancer treatment

Different microbial toxins such as lipopolysaccharide endotoxin, brevetoxins, microcystins, etc., are inactivated by titanium dioxide photocatalyst. A photocatalyst such as TiO₂ can kill a wide range of microorganisms including fungi, algae, viruses, and even cancer cells. TiO₂ photocatalyst does not inhibit the reproduction of bacteria only, but also it simultaneously decomposes the bacterial cells under mild conditions [99].

2.3.3. Self-sterilization

The photocatalyst is chemically activated by light energy, and decomposes the pollutants and different types of typical pathogenic organisms such as bacteria, viruses, fungi, and so on, from water, air and surfaces under sunlight irradiation. Due to their physical and chemical stability and their safety as materials, these photocatalyst and especially the titanium dioxide has been used as an additive for food and cosmetics [100, 101].

2.3.4. Water splitting

Overall water splitting to produce H_2 and O_2 over a semiconductor photocatalyst using solar energy is a promising process for the large-scale production of clean, recyclable H_2 (see figure 4). Numerous attempts have been made to develop photocatalysts that function under visible-light irradiation to efficiently utilize solar energy. A number of oxides and sulfides have been used as photocatalysts for water-splitting reactions. TiO_2 and many coupled semiconductors such as $CaFe_2O_4/TiO_2$ offer a promising way to produce hydrogen from water [102-104].

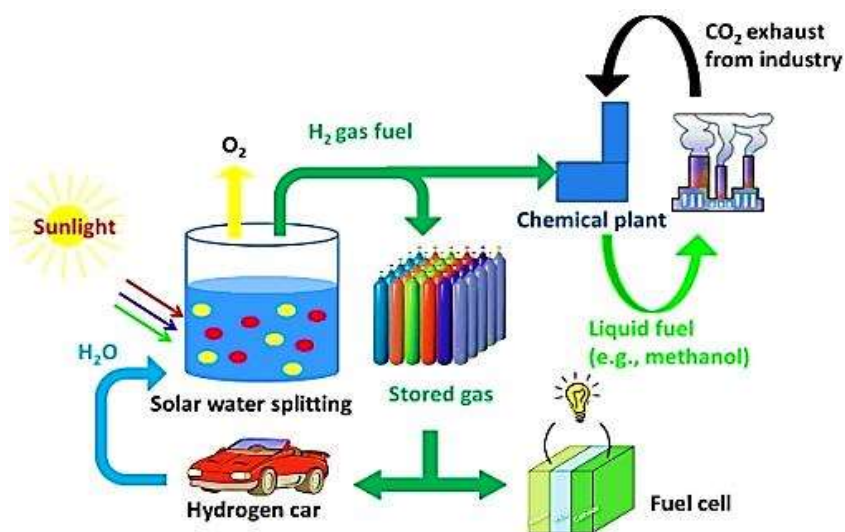


Figure 4: photocatalytic water splitting [256].

2.3.5. Water treatment

Many semiconductors from metal oxides and sulfides have been used as photocatalysts in waste water treatment. Titanium dioxide and zinc oxide photocatalysts are the most commonly used in waste water purification [105, 106, 107].

2.3.5.1. Photocatalytic materials

For the development of a photocatalyst, there are few basic materials requirements. Most of the semiconductors have been used in the past to design and obtain efficient photocatalysts. There are many important things to do so. The first and most important is the band gap absorption by the semiconductor material, because it is known that the visible light exhibits only around 42% of the total solar spectrum. This visible spectrum has an energy range between 2.43 eV to 3.2 eV [108]. Thus, a design of a semiconductor that has band-gap energy in the visible region of the solar spectrum is a need. Figure 5 shows the band gap energy values for some semiconductors used in the photocatalytic process. The semiconductors that have an UV band gap are less suitable for the photodegradation mechanism of pollutants compared with that of visible band gap semiconductors.

The second important parameter is the position of the valence band VB and conduction band CB. The valence band should be lower than the oxygen oxidation potential and the conduction band should be higher than the hydrogen reduction potential [109]. Most of chemical pollutants are dissolved in water and water splitting will take place at 1.23 eV. Thus, to produce a big number of photoelectrons, the band gap position of semiconductors should be higher than the energy required for water splitting. In other word, the band edge of CB should be higher than the reduction potential of hydrogen, and the VB position should be lower than the oxidation potential of water (see figure 5).

The other material requirements with respect to semiconducting and electrochemical properties are:

- The capacity of separating photo-excited electrons from reactive holes,
- Minimizing of energy losses related to charge transport and recombination of photo-excited charges,
- Chemical stability against corrosion and photocorrosion in aqueous medium,
- Kinetically suitable electron transfer properties from photocatalyst surface to water,
- Being easy to synthesize and cheap to produce.

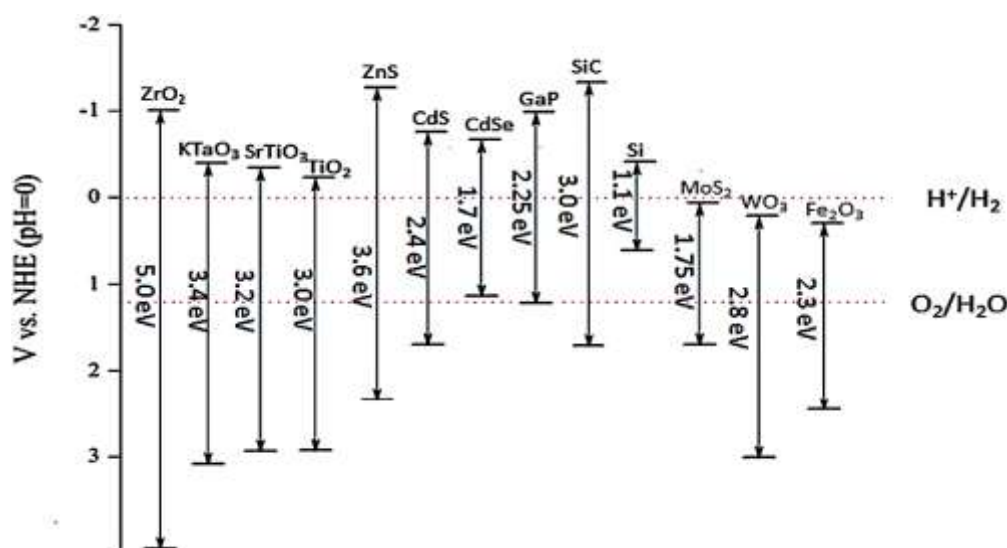


Figure 5: Band positions of some semiconducting materials [257].

2.3.5.2. Mechanism

The first studies of the concept of the heterogeneous photocatalysis are those reported by Doerfler and Hauffe, published in 1964 when they were carried out the oxidation of CO using zinc oxide as catalyst under illumination.

The photocatalytic oxidation steps of organic pollutants by a photocatalyst can be explained as shown in Fig. 6 [110]:

1. Organic pollutants diffuse from the liquid phase to the surface of the photocatalyst.
2. Adsorption of the organic pollutants on the surface of the photocatalyst.
3. Oxidation and reduction reactions in the adsorbed phase.
4. Desorption of the products.
5. Removal of the products.

When the photocatalyst is photo-induced by solar light with photonic energy ($h\nu$) equal to or greater than the excitation energy, it will produce pairs of electrons (e^-) and holes (h^+). The electron of the valence band (VB) becomes excited when illuminated by solar light to the conduction band (CB) of the catalyst therefore creating the negative-electron (e^-) and positive-hole (h^+) as shown in (Eq. (1)). This stage is referred as the semiconductor's photo-excitation state, and the energy difference between (VB) and (CB) is known as the Band Gap (see figure 5).

The electron-hole pairs can migrate to the surface of the photocatalyst and then be involved in redox reactions as shown in (Eqs. (2) – (4)), wherein the h^+ reacts with water and hydroxide ions to produce hydroxyl radicals while e^- reacts with oxygen to produce superoxide radical anions $O_2^{\bullet-}$ then hydrogen peroxide (Eq. (5)). Hydrogen peroxide will then react with superoxide radicals to form hydroxyl radicals OH^{\bullet} (Eqs. (7) – (9)). Then, the hydroxyl radicals will attack the pollutants adsorbed on the surface of the photocatalyst to produce intermediate compounds, these intermediates will be then converted to green compounds such as CO_2 , H_2O and mineral acids as shown in (Eq. (11)). Noting that the hydroxyl radical is the most reactive agent and is one of the most potent oxidizing agents next to fluorine it can remove electrons from any molecule present in

its path, turning that molecule into a free radical [111, 112]. It should be noted that some of the electron-hole pairs will undergo recombination, which reduces the quantum yield. This recombination rate is affected by many factors related to photocatalyst structures and surface modifications [113, 114].

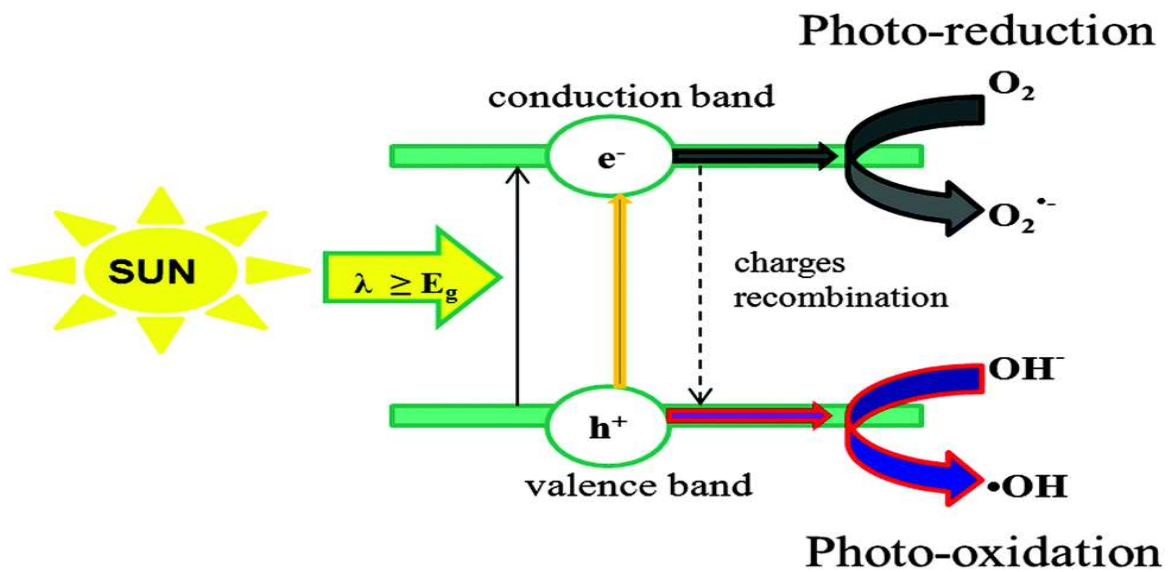
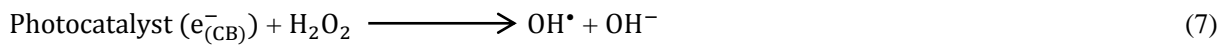
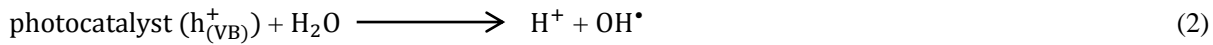
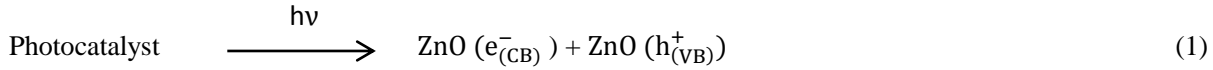


Figure 6: Mechanism of the photocatalytic reaction [258].

Mechanism of the photodegradation of phenol:

The first step mechanism for the direct photolysis of phenol is shown in equation 1:



In the presence of oxygen, the reaction of phenoxyl radicals with O₂ will most probably result in the formation of benzoquinone (equation 2), but the reaction rate is very small.



The reaction of phenol with OH radicals leads to the formation of dihydroxyl cyclohexadienyl radicals (equation 3). In the presence of oxygen, subsequent reaction of the dihydroxyl cyclohexadienyl radicals leads to the formation of peroxy radicals by the addition of molecular oxygen (equation 4). Peroxy radicals are known to form hydroquinone and catechol after eliminating superoxide radicals and rearranging the aromatic system (equation 5). These compounds further degrade into biodegradable products such as carboxylic acids (equation 6).



Chapter 3: Synthesis of zinc oxide nanorods

Several semiconductor oxide materials such as zinc oxide (ZnO), titanium dioxide (TiO_2), strontium titanate (SrTiO_3), tin oxide (SnO_2) and tungsten oxide (WO_3) etc. are known as good photocatalysts [115-118].

Among these semiconductors the use of zinc oxide (ZnO) as a semiconductor photocatalyst is preferred because it has various favorable properties, including good transparency, high electron mobility, and a comparable band gap (3.37 eV) [119, 120] with relatively large quantum efficiency in comparison to the other oxide photocatalysts. Also, it has great potential applications due to its high chemical stability, good photoelectric and piezoelectric behaviors. Furthermore the production cost of ZnO nanoparticles is up to 75% lower than that of TiO_2 and Al_2O_3 [121].

3.1. Classification of ZnO and choice of structure

Nanostructures of zinc oxide photocatalyst can be divided into zero-dimensional (0D), one-dimensional (1D), two-dimensional (2D) and three dimensional (3D), which can be subdivided into quantum dots arrays, elongated arrays, planar arrays and ordered structures respectively (see figure 7).

The 1D ZnO arrays include: nanorods, nanofibres, nanowires, nanotubes and nanoneedles. Nanosheets and nanoflowers are examples of ZnO nanostructures in 2D and 3D arrays respectively. The photocatalytic degradation activity of a photocatalyst is affected by its specific surface area, therefore enabling more contaminants to be adsorbed onto its active surface and thus lead to more pollutants being attacked by hydroxyl radicals [122]. In comparison with the other ZnO nanostructures, 1D ZnO have unique characteristics of increased surface area, advanced geometric structures, specific morphology and atomic arrangements, dense network, and favorable electron transportation. These advantages are linked to the functional properties of ZnO [123]. ZnO NRs have been proved to possess great photocatalytic activity. NRs could act better than their particle form. Sunandan et al [124] have compared ZnO nanorods exposed surface area to the organic contaminants. As shown in figure 8, the nanoparticulate thin film showed minimum activity (degradation efficiency of 64% after 180 min; $k = 0.005993 \text{ min}^{-1}$). Sample 2 with the maximum surface area (47.54 cm^2) gave the highest activity (degradation efficiency of 90%; $k = 0.012792 \text{ min}^{-1}$) and sample 1 with the minimum surface area among the nanorod samples (34.27 cm^2) had the lowest activity (degradation efficiency of 78%; $k = 0.008412 \text{ min}^{-1}$). Thus, was the choice of ZnO NRs to be the best candidate in the photocatalytic experiments. Table 1 shows the advantages and disadvantages of different zinc oxide nanostructures in photocatalytic applications [125].

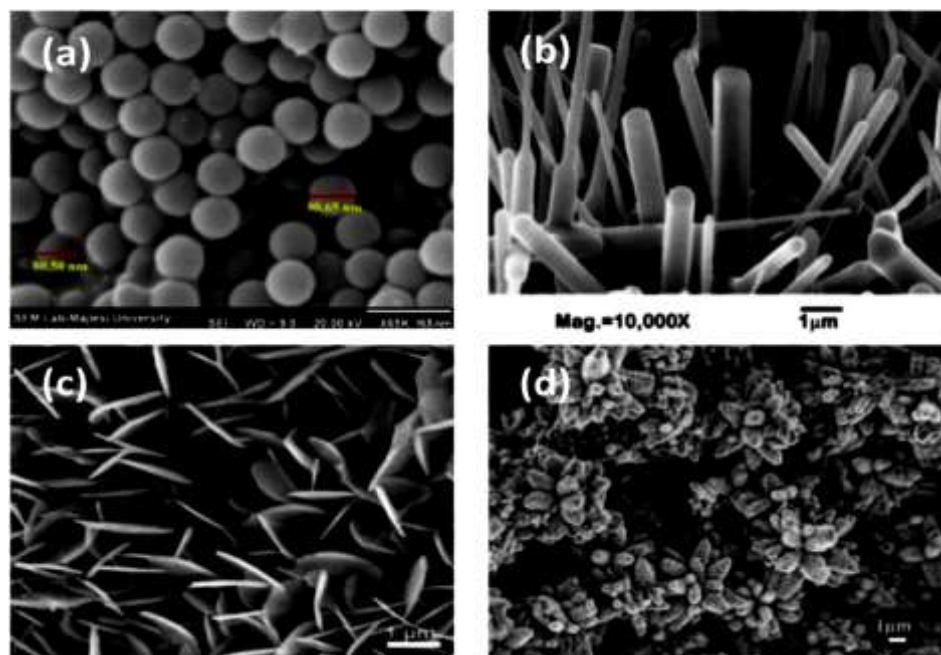


Figure 7: FESEM and SEM images for (a) 0D, (b) 1D, (c) 2D, (d) 3D zinc oxides [259].

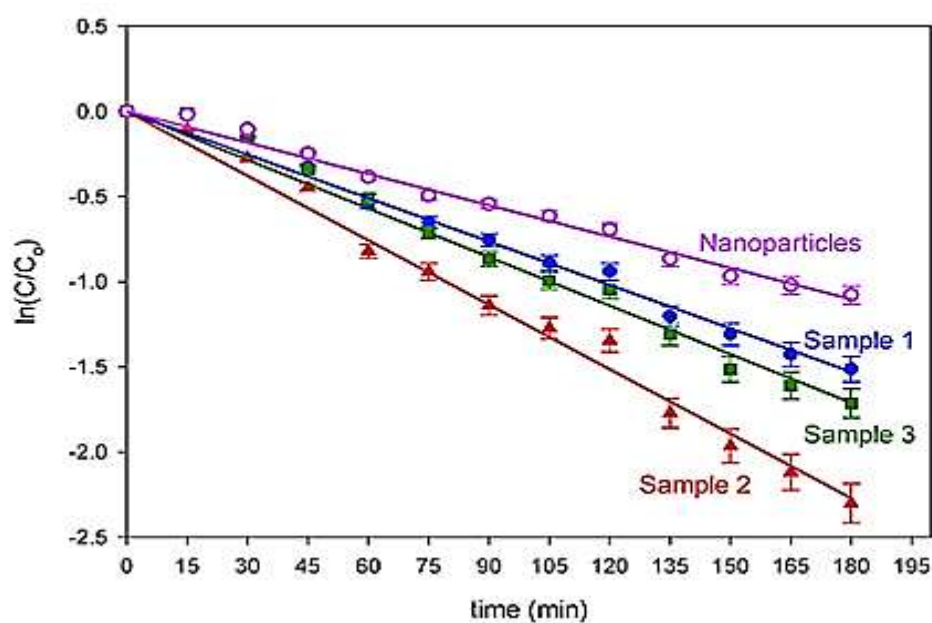


Figure 8: Photocatalytic degradation of methylene blue using ZnO nanoparticles and nanorods on glass substrates upon excitation with light from a tungsten halogen lamp (~72 klux) [260].

	Advantages	Disadvantages
Nanoparticles	Can be easily suspended in a solution. Outstanding performance owing to their large surface areas.	Easily form agglomerates in solution, which contributes to reduced effective surface area. Post-treatment for catalyst removal is required. Complete recovery of catalyst is difficult.
Nanowires	Growth could be easily carried out on most substrates. Consists of large effective surface area compared to nano-thin films. Post-treatment to remove catalyst is not required. Lower crystallinity and more defects.	Growth conditions are highly restricted. Lower surface area compared to nanoparticles.
Nano-thin film	Can be coated on certain substrates. Post-treatment to remove catalyst is not required.	Performance is restricted by small surface area.

Table 1: Advantages and disadvantages of different ZnO nanostructures used in the photocatalytic applications [259].

3.2. Synthesis techniques of Zinc oxide nanomaterials

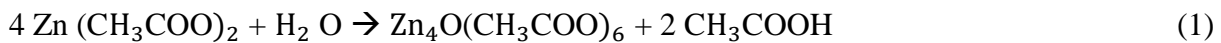
There are various techniques for the synthesis of zinc oxide nanostructures. These synthesis methods can be divided into solution-based and vapor phase approaches. Among ZnO nanomaterial synthesis approaches, the solution-based method is the simplest and least energy consuming. Through this synthesis technique, the morphology of the nanostructures can be easily controlled by manipulating the experimental factors such as type of solvents, starting materials and reaction conditions [126]. This approach also offers better control of the sizes of nanostructures. The solution-based approach to synthesize ZnO nanostructures include: hydrothermal, sol-gel, precipitation, micro-emulsion, solvothermal, electrochemical deposition process, microwave, wet chemical method, flux methods and electrospinning [127- 137]. Among these methods, the hydrothermal technique is very attractive to prepare nanoparticles with the desirable photocatalytic properties due to its simplicity, cost effectiveness, environmental friendliness, and also it provides better control over morphology of the photocatalyst nanostructures and orientation of the nanorod array films [138, 139].

On the other hand, vapor phase techniques have also been used to produce nanostructured materials; these approaches include: thermal evaporation [140], pulsed laser deposition [141], chemical vapor deposition [142], physical vapor deposition [143], metal-organic chemical vapor deposition (MOCVD) [144], plasma enhanced chemical vapor deposition (PECVD) [145] and molecular beam epitaxy (MBE) [146]. These approaches uses gaseous environment and normally the synthesis of nanostructured materials is carried out at high temperatures (ranging from 500°C to 1500°C). Thus, due to the high synthesis temperature, it is most economical and practical to focus on the solution-based techniques.

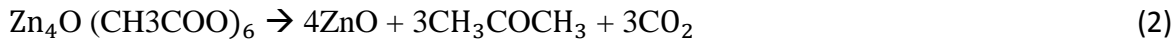
3.2.1. Nanorods growing procedure

a) Role of seeding

Seeding can be carried out by processes such as dip coating, spin coating [147], slip casting, aerosol spraying, chemical vapor deposition, physical vapor deposition, spray pyrolysis, reactive sputtering, electrochemical deposition, plasma spraying, etc. These coating techniques would result in photocatalyst thin-films of various thicknesses and morphologies. Nevertheless, seeding through spray pyrolysis method was found as the simplest, economical and effective in terms of rod's attachment to the substrates. Seeding of the substrates in all the experiments was done with the use of zinc acetate dehydrate $\text{Zn}(\text{CH}_3\text{COO})_2$ as precursor, in which it was dissolved in Deionized water, and then sprayed on the preheated glass substrates. The zinc acetate is known to decompose at a temperature of 237 °C [148] through the formation of basic zinc acetate arising from the loss of acetic anhydride. Acetic anhydride further hydrolyses to form acetic acid as in Eq. 1.



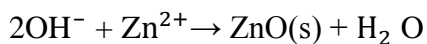
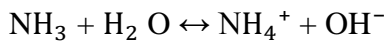
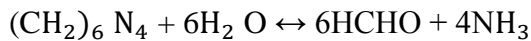
When the temperature of the reactant solution is increased to about 300 °C, decarboxylation occurs and basic zinc acetate decomposes to its oxide leading to the formation of ZnO nanocrystallites, as shown in Eq. 2 [149].



Thereby, a post annealing temperature of 350 °C was chose in all experiments, noting that the higher the preheating temperature is the higher the formation of crystallized clusters, but there is a limit above it the substrate will crack.

b) Role of precursors

Therefore, to grow the rest of the nanorods, hexamethylenetetramine (HMT) which is a highly water soluble, non-ionic tetradentate cyclic tertiary amine and Zinc nitrate hexahydrate ($\text{Zn}(\text{NO}_3)_2 \cdot 6\text{H}_2\text{O}$) were used. Thermal degradation of HMT releases hydroxyl ions which react with Zn^{2+} (from $\text{Zn}(\text{NO}_3)_2 \cdot 6\text{H}_2\text{O}$) ions to form ZnO. This can be summarized in the following equations:



3.2.2. Effect of growing parameters on the photocatalytic activity

a) Precursor concentration

The concentration of the precursor solution affects the growth rate of ZnO nanorods. Depending upon the availability of Zn^{2+} ions, the growth initially occurs uniformly both laterally as well as longitudinally [150]. Because of the polarization vector which is directed along the c-axis of ZnO nanomaterial, longitudinal growth is thereby much faster than the lateral growth. At this stage, the majority of the growth units have easy access to the polar (0001) plane of the growing crystal; consequently, the crystal grows only along the c-axis. This linear growth causes the aspect ratio of nanorods to increase faster. On the other hand, precursor concentration has also a strong influence upon the density of ZnO NRs [151]. This is because in a concentrated precursor, a large number of growth units can manage to adsorb onto the ZnO seeds through heterogeneous nucleation.

b) Hexamine to zinc nitrate relative concentrations

The role of hexamine in the hydrothermal synthesis is to provide OH^- anions for the formation of $\text{Zn}(\text{OH})_2$ which forms the building blocks for the ZnO nanorod growth. The 1:1 molar ratio of zinc nitrate and hexamine in the precursor solution has been reported to produce good quality nanorods [152]. Thus, equimolar concentration of hexamine and zinc nitrate hexahydrate had been used in the precursors in all the experiments.

c) Effect of PH

In the photocatalytic reactions, the PH of the solution is a vital factor, because it makes a clear explanation on the surface charge properties of the photocatalyst. A change in PH affects the efficiency of the degradation of the photocatalyst.

As can be seen in Figure 9, increasing pH value of the dye suspension caused exponential increase in the photocatalytic degradation of MB suspension. The reason could be the high concentration of free OH^- anions that are converted into hydroxyl radicals (OH^\bullet) which is a dominant oxidizing agent in photocatalysis [153], through oxidation reactions initiated by the photogenerated holes (h^+).

d) Calcination temperature

The study of the effect of the reaction temperature is important. The figure 10 shows the variation in the visible emission peak from ZnO NRs annealed at 150°C, 250°C, 350°C and 450°C respectively. For annealing temperatures up to 250°C, the intensity of the green emission was found to increase. This trend has been primarily attributed to the migration of oxygen vacancy states from the bulk towards the surface of the NRs [154], resulting in a relative increase in the surface defect states concentration, which is maximum for the 250°C annealed ZnO NRs. Annealing the NRs further can passivate the surface defects and thus leads to a reduction of the green emission [155].

Figure 11 shows the photocatalytic degradation profile of MB under visible light irradiation with ZnO NRs annealed at different temperatures. The rate constants of MB photocatalytic degradation with differently annealed ZnO NRs are shown in Fig. 11 b. An increase in the MB degradation rate constants was observed with increasing annealing temperatures up to 250°C, the degradation was found to be lower upon annealing at temperatures higher than 250°C. This clearly suggests a direct relationship between visible light photocatalytic activity and surface defects on zinc oxide NRs.

Typically defect states improve the optical absorption by allowing sub-band gap transitions and thereby generating active e-h pairs under visible light irradiation [156, 157-160], which can be transferred to the surface adsorbed MB molecules, thereby, increasing the electron transfer rate with increasing surface defects [161]. However, the ZnO NRs annealed at temperatures higher than 250°C showed reduction in their photocatalytic degradation rate and this is due to the reduction in the surface defects that in turn limits the electron transfer process from ZnO surface defects to MB molecules.

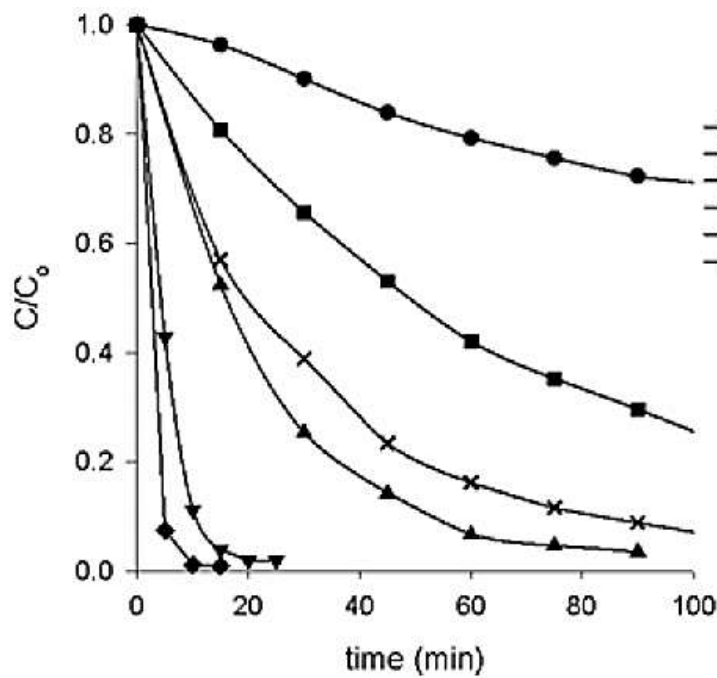


Figure 9: Normalized concentration against irradiation time when 5 μ M aqueous [261].

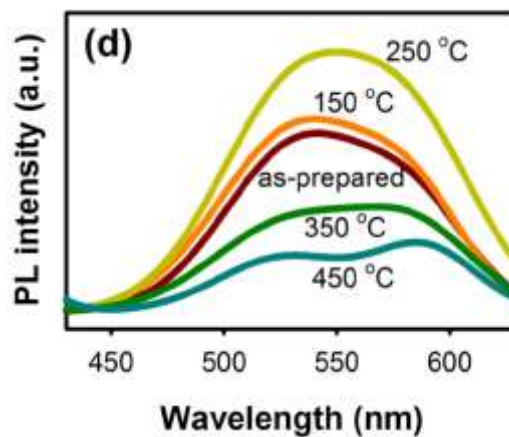


Figure 10: variation in the visible emission peak from the ZnO NRs annealed at different temperatures [262].

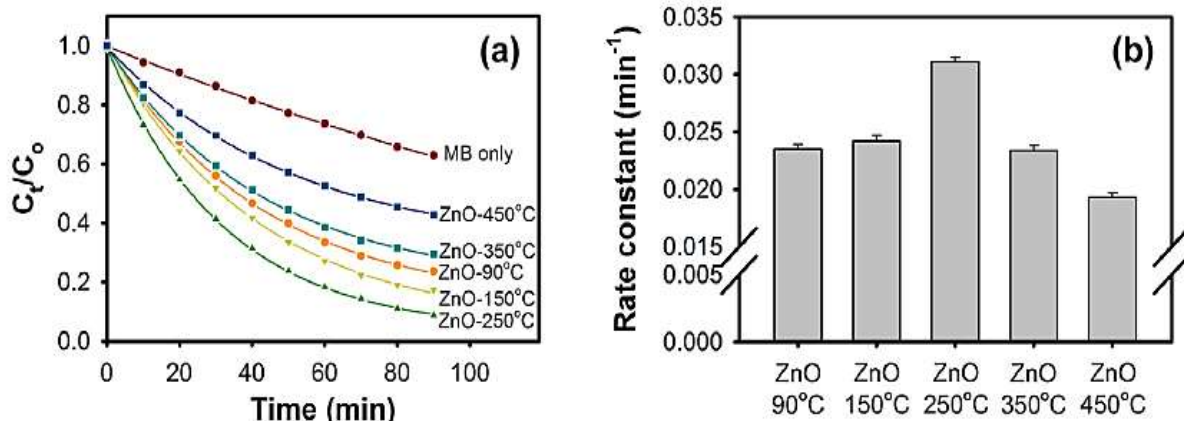


Figure 11: Photocatalytic degradation profile of 10 mM methylene blue (MB) in aqueous solution under visible light irradiation with ZnO NRs photocatalysts annealed at different temperatures (90, 150, 250, 350 and 450 °C for 1 h). (a) Degradation kinetics of MB; (b) degradation rate constants of MB [262].

e) Effect of amount of catalyst

The amount of the catalyst in the photocatalyst also influences the efficiency of photocatalytic degradation. If there is an increase in the quantity of catalyst, the number of active sites on the semi-conductor surface increases moreover, which in turn produce a greater number of OH^\bullet and $\text{O}_2^{\bullet-}$ radicals. As a result, the photocatalytic degradation rate is increased. The degradation rate is directly proportional to the catalyst's concentration in any reactor system. However, if the catalyst loading is improved beyond an optimum concentration, the degradation rate is then unfavorable because there will be a decrease in the light penetration depth into the solution and consequently diminishing of light scattering occurs.

f) Effect of light intensity

The efficiency of the photocatalytic reaction mostly depends on the light intensity. The quanta of light absorbed by any photocatalyst are given by the quantum yield which is the ration of the rate of reaction to the rate of absorption of radiation. The responses of the photocatalytic reaction varied under different wavelengths of light source. The degradation reaction rate of the photocatalyst varies for different intensities of light; the reaction rate increases with increasing light intensity. The reaction rate decreases at high-intensity light radiation because the excessive light intensity promotes more electron-hole recombination.

g) Effect of irradiation time

The photodegradation of the pollutants varies with the time of irradiation. The photocatalytic activity of the photocatalysts nanoparticles and photodegradation of the pollutant increases with respect to the light irradiation time. This can be related to the amount of photogenerated electron-hole pairs which are produced due to the sensitization of photocatalyst nanoparticles.

h) Concentration and nature of pollutants in wastewater

Another main factor that affects the degradation rate is the pollutant type and their concentration. A number of studies have reported the dependency of the concentration of pollutants in water on the photocatalyst reaction rate. High concentration of contaminants in water saturates the surface of the photocatalyst therefore reduces its photonic efficiency and deactivates the photocatalyst. In addition to the concentration of pollutants, the chemical structure of the target contaminant also influences the degradation performance of the photocatalytic reactor. For example, 4-chlorophenol requires prolonged irradiation time due to its transformation to intermediates compared with oxalic acid that transforms directly to carbon dioxide and water.

In other words, the photocatalytic degradation of aromatics is highly dependent on the substituent group. The organic substrates with electron withdrawing nature (benzoic acid, nitrobenzene) strongly adhere to the photocatalyst and therefore are more susceptible to direct oxidation compared with the electron donating groups.

3.3. ZnO properties affecting the photocatalytic process

The photocatalytic activity of the metal oxides nanomaterials depends on various factors such as composition, particle size, crystallinity, surface defects, etc.

a) Defects in ZnO

The defects in the semiconductor photocatalyst can be vacancies, interstitials or substitution type defects. These defects create intermediate electron and hole traps between the valence band (VB) and conduction band (CB) leading to a reduction of energy required for exciton pair generation, rendering the materials more visible light active [162,163] and reducing the recombination of the photogenerated electron-hole pairs. Moreover, the photogenerated holes trapped by surface defects are ready to react with electron donors leading to the formation of O_2^- , OH^\bullet and other oxygenated radical species which are very effective in degrading contaminants in water [164, 165], thus, increasing the photocatalytic activity of the semiconductor photocatalysts (see figure 12).

In ZnO photocatalysts, oxygen vacancies and zinc interstitials are two predominant intrinsic defects which are reported to be favorable for photocatalysis [166–168]. The formation of these defects is generally governed by the synthesis environment, where a zinc rich environment typically leads to oxygen vacancies and zinc interstitials and an oxygen rich environment leads to zinc vacancies and oxygen interstitials [169-171].

In fact, the roles of the defects on ZnO nanomaterials in absorption and surface reactivity have been extensively acknowledged [172–174]. Zheng et al. showed that the oxygen defects (oxygen vacancies and interstitial oxygen) that formed in a solvothermal process had an impact on the photocatalytic activity of ZnO [174]. Wang et al. developed enhanced the visible light photocatalytic activity of ZnO by narrowing the band gap with defects [172]. Li et al. reported that a good concentration ratio of bulk defects to surface defects in TiO₂ nanocrystals can improve the separation of photogenerated electro-hole and therefore can enhance photocatalytic efficiency [175].

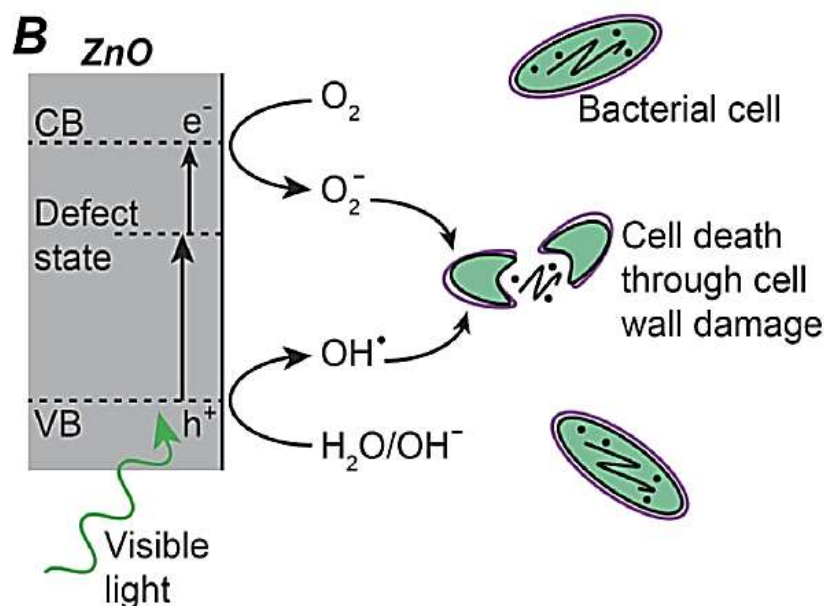


Figure 12: Schematic representation for the mechanism of antibacterial activity of ZnO NRs [262].

b) Particle morphology

In general, the difference in photocatalytic activity is related to size and surface area of the semiconductor photocatalyst. Recently, Jang et al. and McLaren et al. have reported the relationship between the exposed surfaces of ZnO crystals and their photocatalytic efficiency, and demonstrated that a greater proportion of exposed polar surfaces lead to a greater photocatalytic activity [176, 177]. One-dimensional zinc oxide nanostructures such as nanorods and nanowires have been investigated extensively and it is proved that they have larger number of e^- and h^+ exist on the active sites of the nanocrystal surface, resulting in higher activity compared with spherical nanoparticles. However, the photocatalytic activity of ZnO depends upon the orientation of the nanorods. The higher photocatalytic activity of nanorods grown with 2 mM precursor, in spite of their small surface area, is due to their random orientations (see Figures 13a and 13d) which exposes maximum surface of the photocatalyst to the incoming light. Contrary to this, NRs fabricated with 40 mM precursor are well aligned and oriented (see Figures 12c and 12f), exhibit lower photocatalytic activity. This is explained by the fact that only tips are exposed to light rays, while a major portion of the side surface of the nanorods remains obscured.

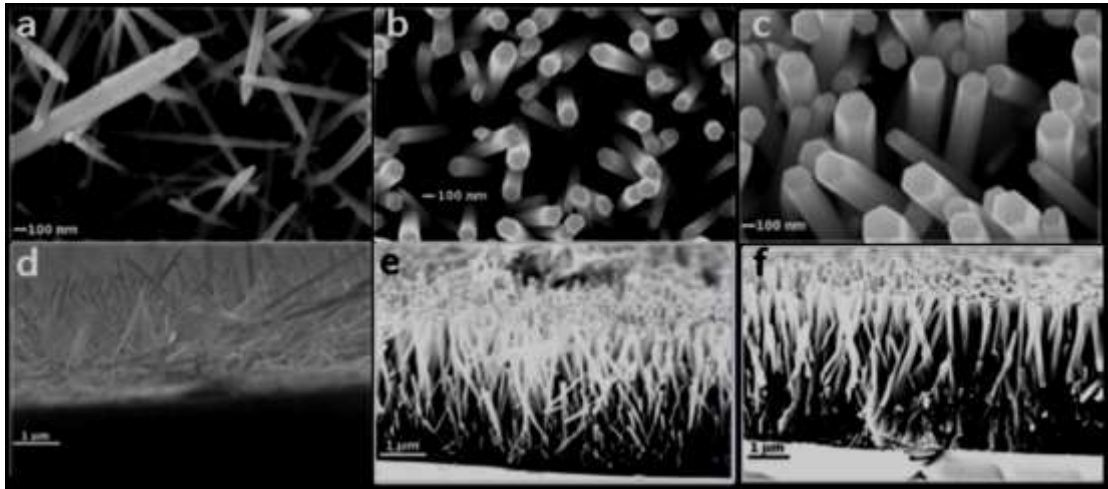


Figure 13: SEM micrographs: (a); (b) and (c) top views; (d); (e) and (f) cross-sectional views of ZnO nanorod arrays grown hydrothermally for 15 h, using precursor concentrations of 2 mM, 10 mM and 40 mM, respectively [261].

3.4. Improvement of ZnO as photocatalyst

The main drawback of ZnO as a photocatalyst is that it absorbs only in the UV region because of its large bandwidth of 3.2 eV. The major problem is that only about 4 to 5% of solar spectrum falls in the UV range. Thereby, researchers developed several techniques to overcome this drawback, such as doping of metal/non-metal atoms, depositing noble metals, and coupling with other semiconductors or carbon materials [177-185].

3.4.1. Doping metals/non-metals

The photocatalytic reactions are mainly governed by band gap energy and hydroxyl radicals. Thereby, doping has been adopted to modify the chemical and physical properties of the zinc oxide nanomaterials by incorporating impurities such as metals or non-metals, to shift the valence band energy of ZnO upward and narrowing its band gap energy to the visible region [186].

Doping metals such as alkali metals (such as Na- or K-doped ZnO) [187,188, 189,190], transition metals (such as Fe [191], Co [192], Ni [193], Mn [194], Cr [195], V [196], Cu [197], and Zr [198]) transition metals, and rare earth metals [199-203] or non-metals such as C, N, and S [204-209, 210,211] NPs can enhance the photoelectric properties of ZnO photocatalyst to extend its spectral response to the visible light region because they can reduce the band gap of the semiconducting materials [212]. The doping metals/non-metals NPs tune the electronic structure of ZnO by adding localized electronic energy level in the band gap (see figure 14). The energy level of the doping atoms is located below the CB of ZnO, where the photogenerated charge carriers are trapped increasing, thereby, the photocatalytic activity of the semiconductor [213-215].

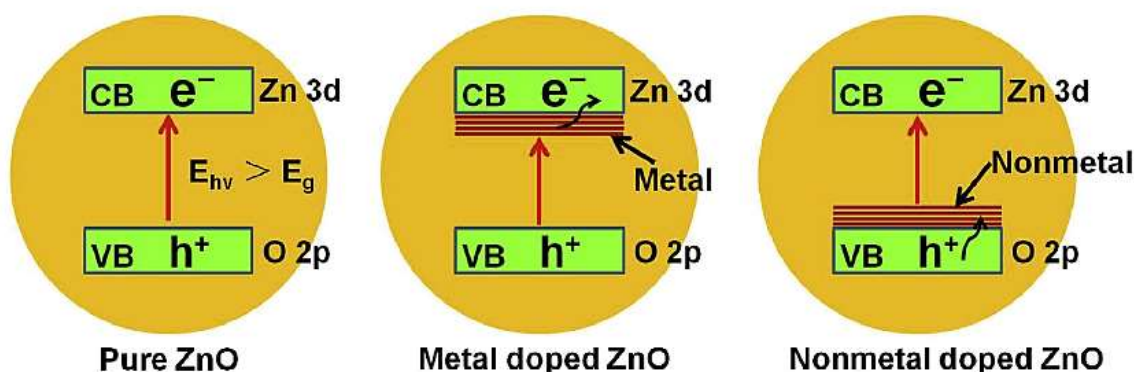


Figure 14: Schematic of the comparison of the band structures of pure, metal-doped ZnO, and nonmetal-doped ZnO.

3.4.2. Depositing of noble metals

The deposition of noble metal NPs can not only modify the reactive sites of ZnO NPs, but also serve as a cocatalyst for the photodegradation of organic contaminants [216]. The study of metal-semiconductor based plasmonic photocatalysts becomes very popular due to the potential of these systems to efficiently utilize the visible light part of the solar spectrum for the photocatalytic degradation of pollutants in water or air [217]. Metal doping of ZnO can improve the photocatalytic activity of the photocatalysts by increasing the trapping site of the photo-induced charge carriers and enhancing the light absorption by ZnO via surface plasmon resonance (SPR). Both effects can decrease the recombination rate of photoinduced electron-hole pairs, facilitate the redox reactions and thus enhance the photocatalytic performance of the photocatalyst [218, 219].

In the recent years, many researchers have reported efficient visible light photocatalysis by using gold (Au) or silver (Ag) NPs deposited on traditional semiconductor photocatalysts like titanium dioxide and zinc oxide [220,221-224]. Incorporation of metal NPs, such as Au and Ag into the semiconductor photocatalysts allow the overall absorption band of the photocatalyst to extend towards the visible region of the solar spectrum, and thus makes the photocatalyst active under both ultraviolet and visible light irradiation, unlike the traditional semiconductors such as ZnO and TiO₂, which absorb the light mostly in the UV region.

Au NPs have been reported to show significant improvement in the visible light photocatalytic activity when incorporated over metal oxide surface [225, 226]. Apart from its good chemical and thermal stability, Au NPs typically form a Schottky type junction when deposited on the surface of traditional metal oxides resulting in efficient charge separation necessary for enhanced photocatalytic efficiency [220, 227]. On the other hand, although silver NPs have relatively lower chemical and thermal stability than gold NPs, the advantages are that Ag is cheaper than Au and it shows superior antimicrobial properties over Au [228-231], which makes it a good and applicable plasmonic material in the photocatalytic design.

3.4.3. ZnO coupling with other semiconductors

Coupling of two semiconductors is an approach that involves coupled semiconductor metal oxides [232]. Thereby, highly active photocatalysts can be obtained by coupling two semiconductors having different band gaps. Nanocomposites are preferable in photocatalysis applications because of their higher light absorption, better suppression of photo-induced electron-hole pair

recombination and increased charge separation. For ZnO photocatalyst coupled with other semiconductors, TiO_2/ZnO , SnO_2/ZnO , $\text{SnO}_2/\text{ZnO}/\text{TiO}_2$ and $\text{Co}_3\text{O}_4/\text{ZnO}$ are the most investigated materials for photocatalytic processes [233-241]. The photogenerated charge separation enhancement mechanism of a $\text{ZnO}/\text{TiO}_{2x}\text{N}_y$ nanocomposite is showed in figure 15. The electron from ZnO NPs was transferred into CB of $\text{ZnO}/\text{TiO}_{2x}\text{N}_y$ whereas the photogenerated hole of $\text{ZnO}/\text{TiO}_{2x}\text{N}_y$ was transferred to ZnO. The occurrence of such phenomena has suppressed the recombination rate of electron-hole pairs by prolonging the life time of charge carriers.



Figure 15: Photogenerated charge separation mechanism of ZnO coupled with $\text{TiO}_{2x}\text{N}_y$ [259].

3.4.4. Coupling of nanocarbon component to ZnO

Coupling of carbon tubes and graphene with ZnO NPs can enhance the photocatalytic activity of the semiconductor. This is due to the fact that the carbon materials can act as a photoelectric reservoir, which stores and shuttles the photogenerated electrons from ZnO to substrates, or perform as photosensitizer, which improves the light absorption of the photocatalyst [242-245]. The loading of graphene can reinforce the photocatalytic activity of ZnO in four steps: (1) speeding up the electron-hole separation and holding them apart, (2) improving the specific surface field because of the SPR, (3) enhancing the absorption of organic pollutants through $\pi - \pi$ combination between the organic pollutants and graphene, and (4) enhancing the light utilization capacity [246].

The figure 16 illustrates the charge transfer pathway during the photocatalytic process over the GQD/ZnO NRs. The GQDs and ZnO NRs were excited by solar light, and the e-h pair was generated in their CB and VB, respectively. Because ZnO is in contact with GQD, the photogenerated electrons in the GQD CB can energetically be transferred to the ZnO CB, and the generated holes in the ZnO VB can energetically transferred to the GQD CB. This process helps in the retardation of recombination of e-h pairs. Thereby, the overall result is the longer separation of e-h pairs and thus, the ability of these e-h pairs to contribute in the photodegradation process.

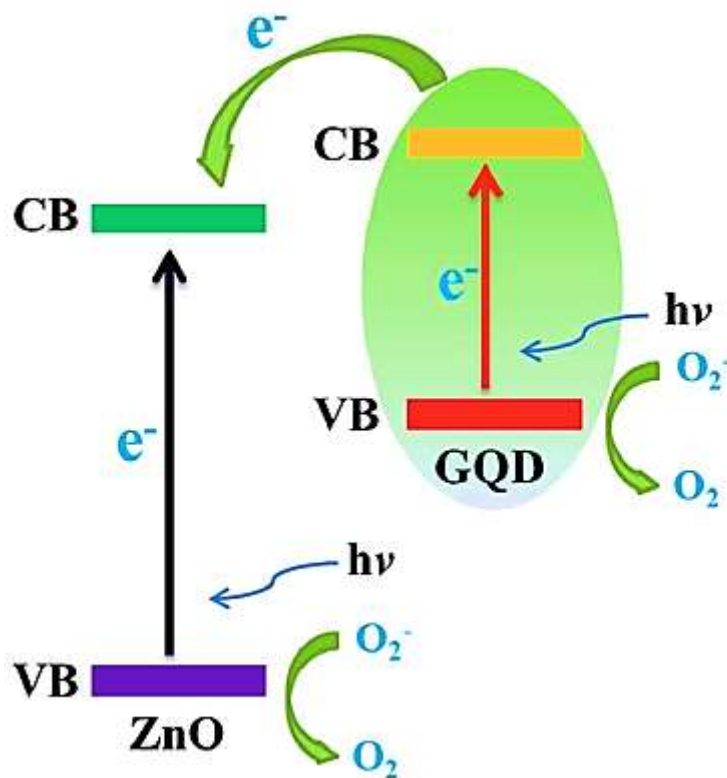


Figure 16: Schematic transfer process of GQDs coated ZNRA.

3.4.5. Crystal growth and shape control

To improve the photocatalytic activity of ZnO NPs, various methods have been used to modify its morphology, size and growth. It has been noted that the photoactivity can be modified by varying the surface lattice plane and surface area of photocatalysts [247]. On the other hand, the morphology of ZnO NPs can be altered by manipulating the molar ratios of precursors [248], because the shape and size of ZnO particles are correlated to the concentration of OH^- ions. The figure 15 shows that low and high concentration of OH^- result in ZnO growth. Also the speed of precursor (sodium hydroxide) being added to the zinc acetate solution could contribute to different growth mechanisms of ZnO nanostructures [249]. A slow addition rate of OH^- leads to a uniform direction growth of ZnO. Otherwise, if both precursor solutions are mixed at the same time, the reaction then will perform faster. In this case, growth along the [0001] direction is more favorable due to the excess of OH^- , leading, thereby, to nanosheet formation. If OH^- is added in a slow rate, the growth along the [0001] direction then will be restricted which leads to the formation of hexagonal prism. Among those different shapes of ZnO nanostructures, spherical ZnO nanostructures exhibits the highest degradation rate of organic contaminants due to their large oxygen vacancies. Effect of ZnO crystallite sizes towards the photocatalytic activity has been well-linked to their band-gap energy [250], in which ZnO crystallite sizes of 4.8 and 31.4 nm are having band-gap energy of 3.29 and 3.18 eV, respectively (see figure 17).

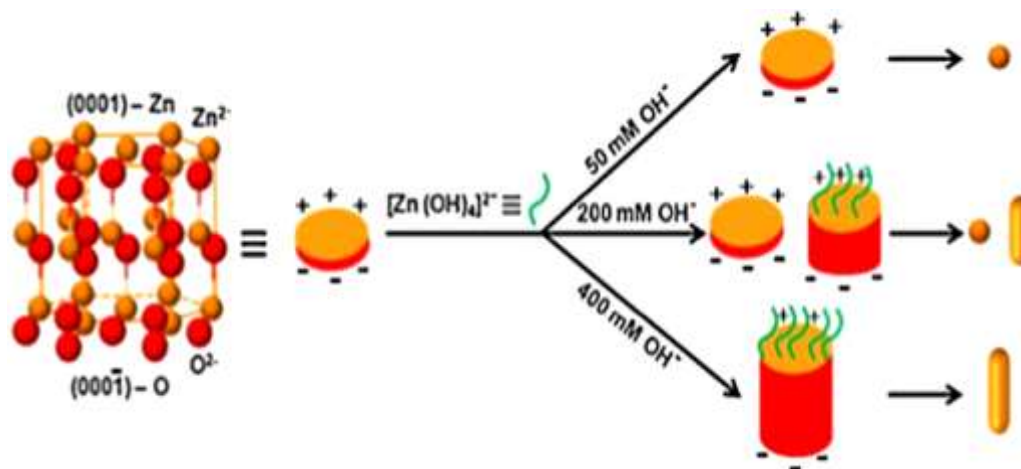


Figure 17: Effect of OH^- concentration towards the mechanisms of ZnO formation [259].

3.4.6. Surface modification of ZnO

Owing to the existence of Zn–O–Zn bonds in ZnO nanoparticles, agglomeration occurs and strongly limiting ZnO nanoparticle applications [251]. Surface modification may be the best approach to ensure better dispersion by preventing the agglomeration of ZnO NPs. In addition, surface modification has also been used to tune the ultraviolet and visible light photoluminescence, as the chemical and physical properties of ZnO nanoparticles can be modified via chemical surface modification through different techniques such as chemical treatment [252] and coating techniques. Chemical treatment is an approach that utilizes coupling agents (e.g. trimethoxyvinyl silane and oleic acid) to modify the surface of nanoparticles.

Chapter 4: Methodology

4.1. Preparation of ZnO nanorods

4.1.1. Materials

- Analytical grade zinc acetate dehydrate ($\text{Zn}(\text{C}_2\text{H}_3\text{COO})_2 \cdot 2\text{H}_2\text{O}$) from MERCK (99% purity), Germany;
- Zinc nitrate hexahydrate ($\text{Zn}(\text{NO}_3)_2 \cdot 6\text{H}_2\text{O}$) from APS Ajax Finechem, Australia;
- Hexamethylenetetramine ($(\text{CH}_2)_6\text{N}_4$) from Aldrich, USA;
- Standard microscope glass slides used as substrates.

4.1.2. Procedure

A hydrothermal growth of ZnO NRs was carried out. First, the substrates were pre-cleaned by successive ultra-sonication in soap water, acetone, isopropanol and deionized water (DI) for 15 minutes each, and then dried for further uses (figure 18 a). Zinc oxide was prepared by dissolving 10mM zinc acetate dehydrate in 25 ml of DI water. Seeding of the substrates in all the experiments was done through spray pyrolysis method in which the prepared solution of zinc acetate was sprayed at a rate of 1 mL/min (from a distance of about 20 cm) on the cleaned substrates pre-heated at 350°C (figure 18 b). The hydrothermal growth of ZnO NRs was carried out by placing the seeded glass substrates in a chemical bath containing equimolar concentrations (20mM) of Zinc nitrate hexahydrate ($\text{Zn}(\text{NO}_3)_2 \cdot 6\text{H}_2\text{O}$) and Hexamethylenetetramine ($(\text{CH}_2)_6\text{N}_4$) (figure 18 c). Then they were placed in a commercial microwave oven (Panasonic, Low Model) for 5 hours, wherein the precursor solution was replenished every 60 minutes. And finally, they were annealed at 250°C to remove any organic residue left on the ZnO NRs surface (figure 18 d).

4.2. Preparation of SnO_2/ZnO NRs composite

4.2.1. Materials

- Urea $\text{CO}(\text{NH}_2)_2$ from MERCK, Germany.
- Ammonium Hexafluorostannate $(\text{NH}_4)_2\text{SnF}_6$, from Aldrich, USA

4.2.2. Procedure

A solution of 0.01 mol/L of $(\text{NH}_4)_2\text{SnF}_6$ in DI water was prepared by dissolving 0.53 g of Ammonium hexafluorostannate in 20 ml of water and stirring to form a clear solution. Another solution of 0.1 mol/L of Urea in Ethanol was also prepared by dissolving 4.8 g of Urea in 80 ml of ethanol. The two solutions were mixed together. Then, the ZnO nanorods coated substrates were

immersed in a bath containing the two mixed solutions already prepared as we described earlier and the bath was heated to 90 °C for 30 minutes. After the reaction took place the nanorods was washed with DI water and dried for further use.

4.3. Synthesis of N-doped GQDs-U

4.3.1. Materials

- Citric Acid Monohydrate $\text{HOC}(\text{COOH})(\text{CH}_2\text{COOH})_2 \cdot \text{H}_2\text{O}$ from J.T.Baker, Holland;
- Urea $\text{CO}(\text{NH}_2)_2$ from MERCK, Germany.

4.3.2. Procedure

2.94 g of citric acid and 2.52 g of urea were dissolved into 70 mL water, and stirred to form a clear solution. Then the solution was transferred into 100 mL Teflon stainless autoclave. The sealed autoclave was heated to 140°C in an electric oven and kept for additional 4 hours. The final product was collected by adding ethanol into the solution and centrifuged at 10 000 rpm for 10 min (see figure 19). The supernatant is then removed, and the residue is washed at least 2 times with water and centrifuged before dipping the ZnO NRs coated substrates with the final residue N-doped GQDs which is easily dispersed into water (see figure 19a).

4.4. Deposition of N- doped graphene quantum dots-Urea on ZnO NRs surface and on SnO₂/ZnO NRs composite

N-doped GQDs-U nanoparticles were deposited in-situ on the ZnO NRs surface and on the SnO₂/ZnO NRs composite surface using the dipping method. The ZnO NRs and SnO₂/ZnO NRs composite coated substrates were immersed in two aqueous solution of N-doped GQDs-U solution for 30 min, 1h, 2h and 3h respectively, with consecutive drying of these substrates for 10 min between these periods (see figure 19 b).



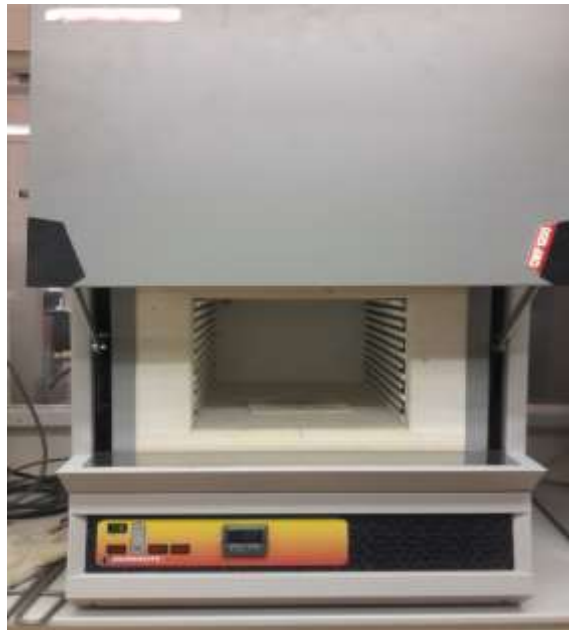
(a)



(b)

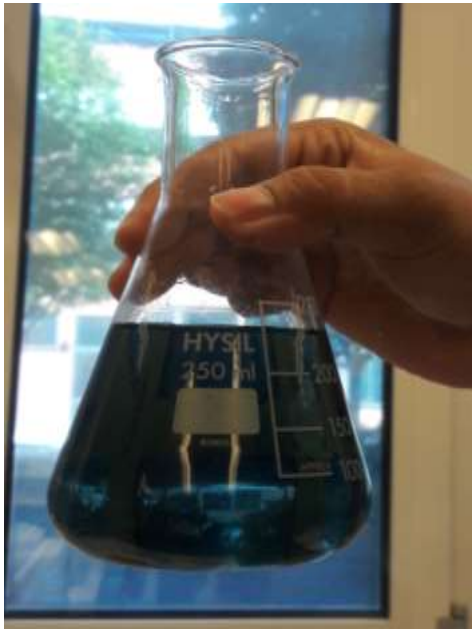


(c)



(d)

Figure 18: (a) Substrates cleaning process in VWR ultrasonic cleaner (b) Seeding the substrates using the spray pyrolysis method (c) Chemical bath of the seeded substrates (d) Annealing of the substrates in an atmospheric furnace at 350°C.



(a)



(b)

Figure 19: (a) N-doped GQDs- U solution (b) ZnO NRs /N-doped GQDs-U substrate

4.5. Characterization

Morphology of the ZnO NRs was characterized by scanning electron microscopy (SEM; Model: JEOL JSM-7600F, Japan) operated at 20 kV. The optical absorption and photoluminescence (PL) spectra of the ZnO NRs, N-GQDs-U and N-doped GQD-U/ZnO NRs were recorded in a UV/Vis spectrometer (Lamda 25 from perkin Elmer, Italy) and a fluorescence spectrometer (LS55 from Perkin, Elmer, Italy) respectively.

4.6. Results and discussion

Scanning electron micrograph (SEM) of the prepared ZnO NRs shows the characteristic hexagonal shape of the NRs with an average length of $\sim 1\mu\text{m}$ and diameter of 200 nm (figure 20).

Figure 21 shows the PL spectrum of ZnO NRs for an excitation wavelength $\lambda_{\text{Ex}} = 320\text{ nm}$, the PL emission is asymmetric implies it has more than one origin. The emission band is characterized by near band emission (NBE-UV) and deep level emission (DLE). The NBE, represent the ultra-violet emission and DLE have a characteristic visible band of violet, blue, green, etc. the DLE bands are divided into intrinsic (native defects) and extrinsic defects. The defects are divided on the bases of their origin:

- Intrinsic defects: origin by one species of atom such as V_{O} (vacancy of oxygen atom), V_{Zn} (vacancy of zinc atom) and Zn_i (zinc interstitial) etc.
- Extrinsic defects: combination of intrinsic sites such as $V_{\text{O}}\text{Zn}_i$

The wavelength corresponds to peak 1: 386.5 nm, peak 2: 403.3 nm, peak 3: 422.8 nm, peak 4: 442 nm, peak 5: 461 nm and peak 6: 485 nm. Each peak corresponds to specific emission which is labeled as mentioned:

1. Peak 1 (UV peak): the UV peak is usually considered as the characteristic emission of ZnO and attributed to the excitonic recombination or near band edge transition. The peak observed at 386.5 nm is attributed to exciton emission i.e. photogenerated electron recombination with the holes in the valence band.
2. Peak 2 (UV-Violet Peak): the peak observed at 403.3 nm is designed as UV-Violet emission arises due to electron transition from conduction band to the acceptor states (singly-ionized oxygen vacancy V_O^+).
3. Peak 3 (Violet-1): the peak located at 422.8 nm is attributed to electron transmission from donor defects (zinc interstitial Zn_i defects) to valence band.
4. Peak 4 (Violet-2): the peak observed at 442 nm is attributed to electron transmission from interstitial Zn_i^+ donor defects to valence band.
5. Peak 5 (Violet-Blue Peak): the peak observed at 461 nm is attributed to electron transmission from doubly ionized zinc vacancy (V_{Zn}^{2-}) donor defects to valence band.
6. Peak 6 (Green Peak): the peak observed at 485 nm is attributed to recombination of shallow trapped (ST) with the acceptor level that resides 0.8 eV above the valence band. Then further electron can relaxed by phonon transition to the ground level.

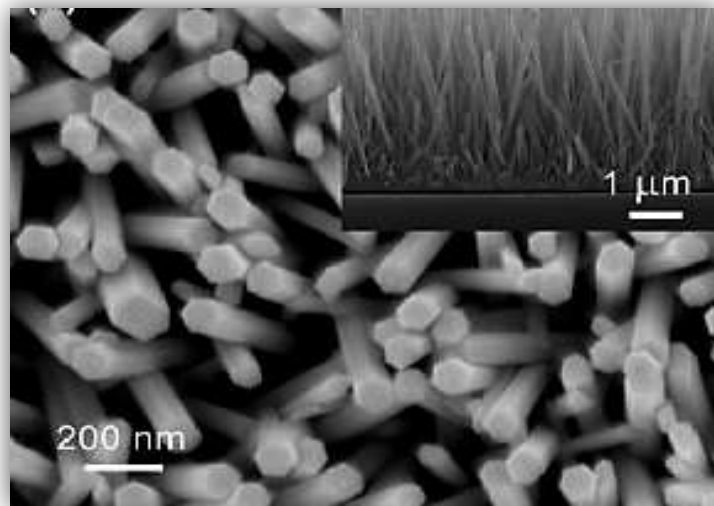


Figure 20: SEM micrographs of ZnO nanorods

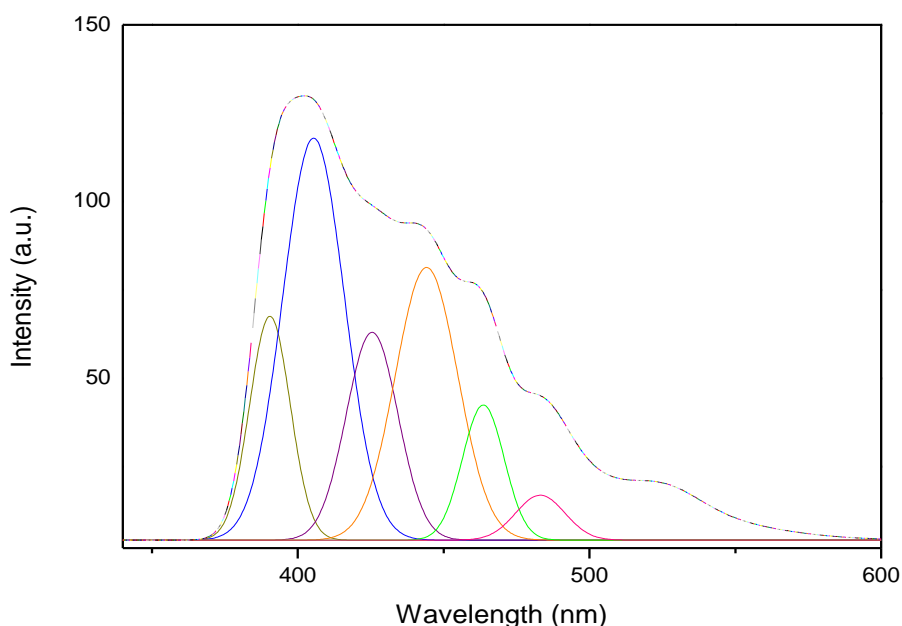


Figure 21: Deconvoluted PL spectra of ZnO NRs for an excitation wavelength $\lambda_{\text{ex}} = 320$ nm

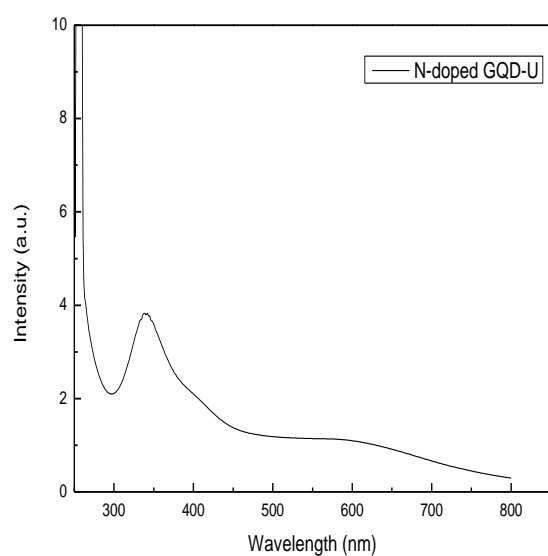
Formation of N-GQDs-U was studied by UV-vis absorption spectrophotometry and photoluminescence spectrometry based on their characteristic peaks and PL emission. Figure 22 shows the UV-vis spectrum of the GQDs suspension in the wavelength range of 200–800 nm. It displays a strong optical absorption peak in the UV region which extends into the visible range. There are two clear absorption bands at 252 nm and 340 nm. The peak seen at 252 nm that corresponds to the $\pi \rightarrow \pi^*$ transition of C=C, and the peak seen at 595 nm corresponds to the $n \rightarrow \pi^*$ transition of C=O bonds in the GDQs. The broad absorption band of N-GQDs observed at 450–600 nm is due to $n \rightarrow \pi^*$ transition of CN bonds. The bandgap energy of the GQDs suspension was calculated as ~ 4.4 eV from the Tauc plot $((\alpha h\nu)^2$ versus $h\nu$ for direct bandgap materials) of its UV-vis absorption spectrum (figure 20b). This large bandgap is an evidence of the formation of GQDs, because graphene has a zero bandgap in theory and when it becomes small enough that quantum confinement effects would dominate, it gains a bandgap.

Further study on the optical properties of GQDs was performed by the PL technique using different excitation wavelengths from 340 nm to 420 nm. As shown in the figure 22c, the increase of excited wavelengths causes a decrease in the PL peak intensity. The figure shows that the photoluminescent emission band did not shift with the change of excitation wavelength. The evolution of the luminescence behavior with a change in the excitation energy is due to the various size distributions and presence of impurity states in graphene quantum dots.

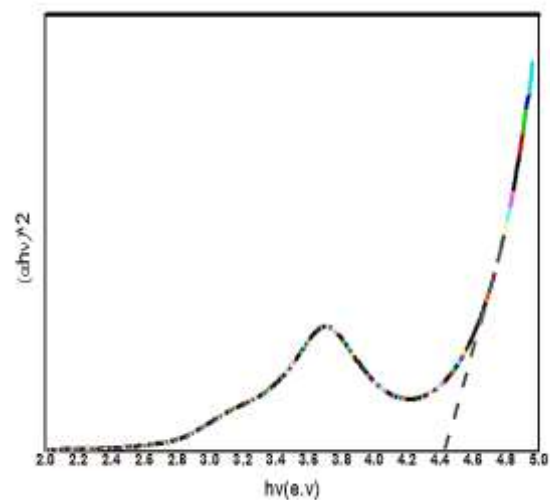
Analysis of photoluminescence spectra can help in understanding the recombination rate of the photogenerated electron-hole pairs, which influences the photocatalytic activity. Figure 23a shows

the absorbance spectra of ZnO NRs and N-GQDS-U/ZnO NRs composites. It shows that the composite exhibits enhanced absorbance in the region between 300 and 500 nm. Figure 22b compares the room-temperature photoluminescence PL spectra of the ZnO NRs and the N-GQDS-U/ZnO NRs composite, excited by the wavelength of 320 nm. As it is seen, in the spectrum related to the N-GQDS-U/ZnO composite, photoluminescence is weaker. The ultraviolet emission band becomes broader and weaker. This decrease in the PL after incorporation of N-doped GQDS-U indicates a large decrease in the radiative recombination rate of electron-hole pairs. In fact, the N-GQDS-U on the ZnO NRs can capture the photogenerated electrons for some time, preventing them to be recombined with their holes counterparts, increasing their chance to be separated from each other and participate in oxidative and reductive reactions. The electron-hole pairs that are not trapped are usually recombined to each other on the order of several picoseconds.

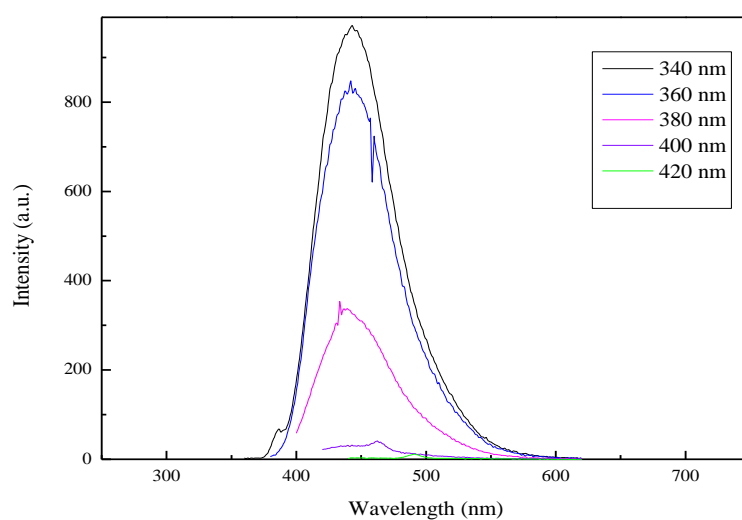
Figure 24 compares the room-temperature photoluminescence PL spectra of the ZnO NRs, the SnO₂/ZnO NRs composite and N-GQDS-U/ SnO₂/ZnO NRs composite, excited by the wavelength of 320 nm. As it is seen, the photoluminescence of ZnO NRs is weaker than the 2 composites. This increase in the PL after deposition of tin oxide on the ZnO NRs indicates a large increase in the radiative recombination rate of electron-hole pairs. In fact, deposition of the tin oxide blocks the defects on the ZnO NRs that was capturing the photogenerated electrons for some time, preventing them to be recombined with their holes counterpart. So after deposition of SnO₂, which has many advantages like protecting the ZnO NRs from dissolution in acidic medium, many electron-hole pairs are not trapped in the defects of ZnO NRs and then are recombined to each other on the order of several picoseconds. After doping the SnO₂/ZnO NRs by N-GQDS-U, the PL become lower, that decrease in the PL after incorporation of N-doped GQDS-U indicates a decrease in the recombination rate of electron-hole pairs in the composite.



(a)



(b)



(c)

Figure 22: (a) UV-vis spectrum of the N-doped GQDs-U suspension (b) tauc plot of the absorption curve of N-GQDs-U (c) Photoluminescence spectra of N-doped GQDs-U.

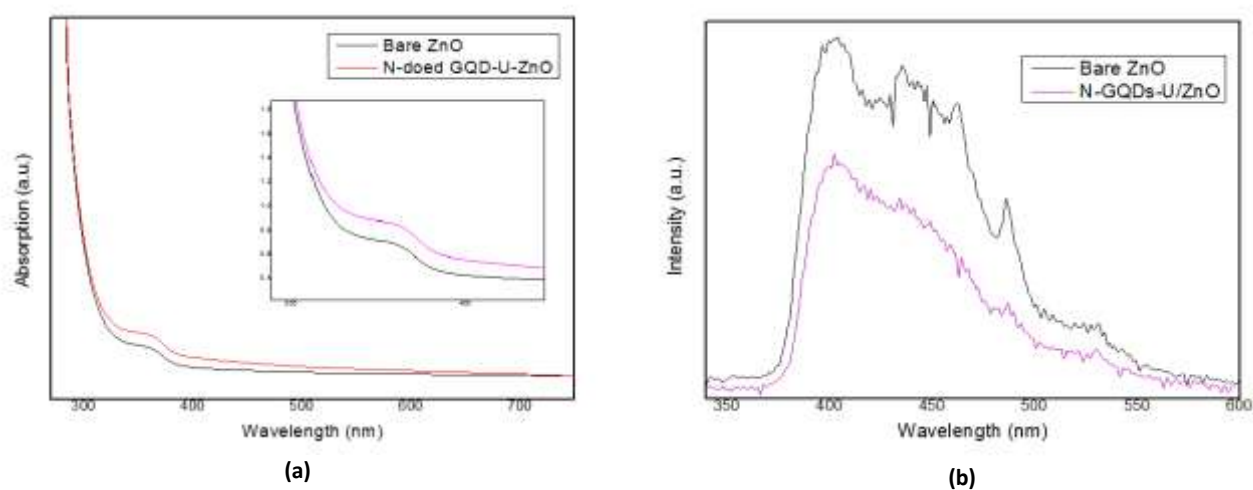


Figure 23: (a) UV-vis absorption spectra of the ZnO NRs and N-GQDs-U/ZnO NRs (b) PL spectra of ZnO NRs and N-doped GQDs-U/ ZnO NRs for an excitation wavelength $\lambda_{\text{Ex}} = 320$ nm

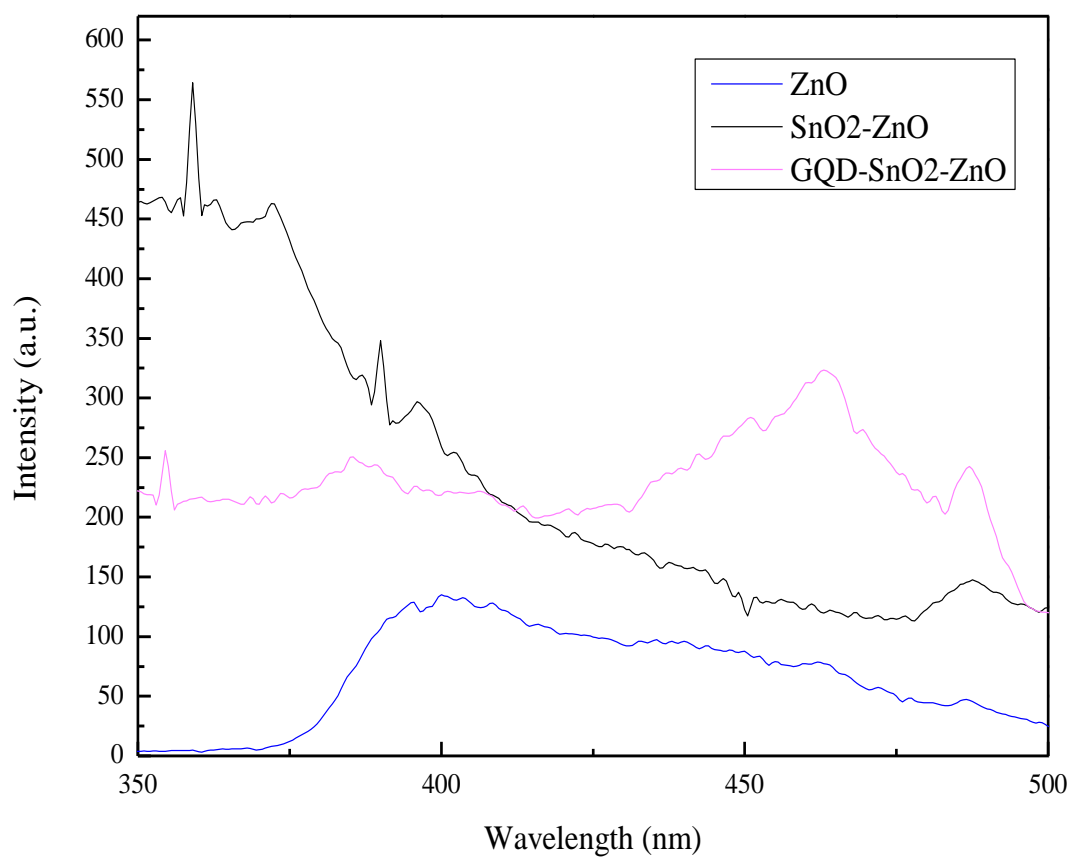


Figure 24: Photoluminescence spectra of the ZnO NRs, the SnO₂/ZnO NRs composite and N-GQDs-U/ SnO₂/ZnO NRs composite for an excitation wavelength $\lambda_{\text{Ex}} = 320$ nm

Photocatalytic test

Methylene blue (MB) was used as a model contaminant for the investigation of the photocatalytic activity of the N-doped GQD-U/ZnO NRs. Low pressure Hg lamp (UVP, San Gabriel, CA 91778 U.S.A.) was used as UV light source and halogen lamp (Co-Tech ECLC-HALO-0103D 150 W) was used as visible light source during the photocatalytic tests. 3.5 ml of 10 μ M aqueous solution of MB was placed in plastic polystyrene VWR Cuvettes PMMA (poly (methyl methacrylate)) macro containing glass substrates (1 cm \times 5 cm) coated with bare ZnO, N-doped GQDs-U/ZnO NRs, SnO₂/ZnO NRs and N-doped GQDs-U SnO₂/ZnO NRs. The photoreactors were kept in dark for 1 h to obtain adsorption-desorption equilibrium, then they were placed under the light of an UV and a visible light halogen lamp for 120 min, in closed area to avoid any hazardous light from other lamps in the surrounding, to conduct the photocatalytic degradation of the MB molecules.

Analytical methods

The photocatalytic reduction of the MB was monitored by recording the optical absorption of the MB solution at 15 min, 30 min, 45 min, 60 min, 90 min and 120 min, respectively, by placing the PMMA Cuvettes in a UV/VIS Spectrometer (Lambda 25 from Perkin Elmer, Italy). The concentration of MB was estimated from the reduction in the absorption intensity of MB at λ_{max} = 665 nm and plotted as C_t/C_0 versus light exposure time, where C_t represents the concentration of MB at time t and C_0 represents the initial concentration of MB.

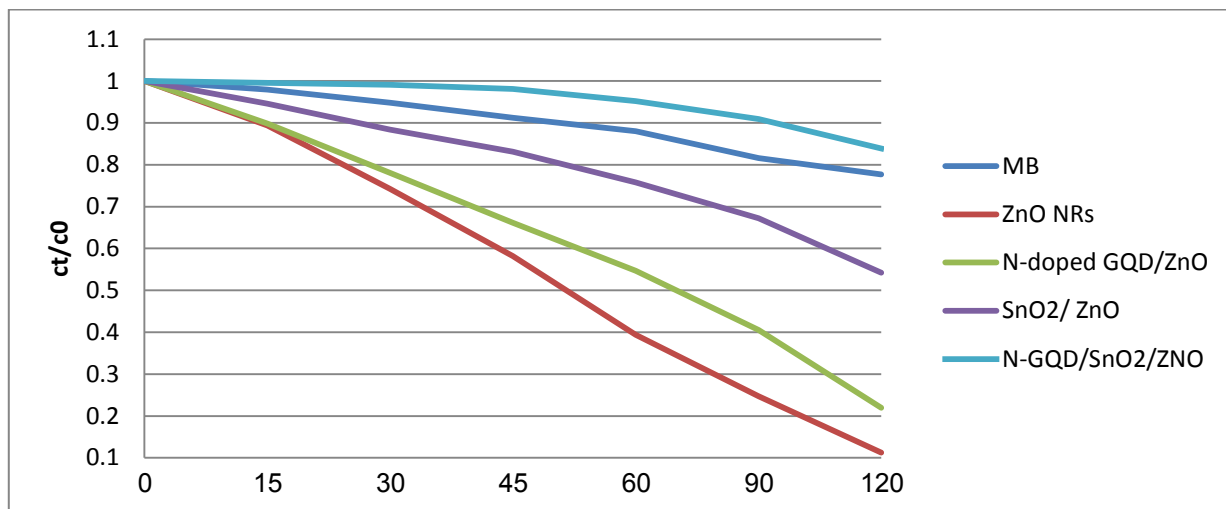
A First order exponential equation ($y = a e^{-bx}$) was used to fit the MB decay curves, where “a” is a pre-exponential factor and “b” represents the degradation rate constant in min^{-1} . Thus, the absorption is measured according to Beer-Lambert law: $A = 3bc$, where A is the absorbance (no unit), 3 is the molar absorptivity with units of $\text{Lmol}^{-1}\text{cm}^{-1}$, b is the path length of the sample, and c is the concentration of the compound in solution, expressed in mol L^{-1} . So, as the concentration c is proportional to the absorbance, we can directly use A/A_0 which is equal to C/C_0 to plot the concentration decay curve. This decay appears to follow the following formula:

$$C/C_0 = a e^{-bt}$$

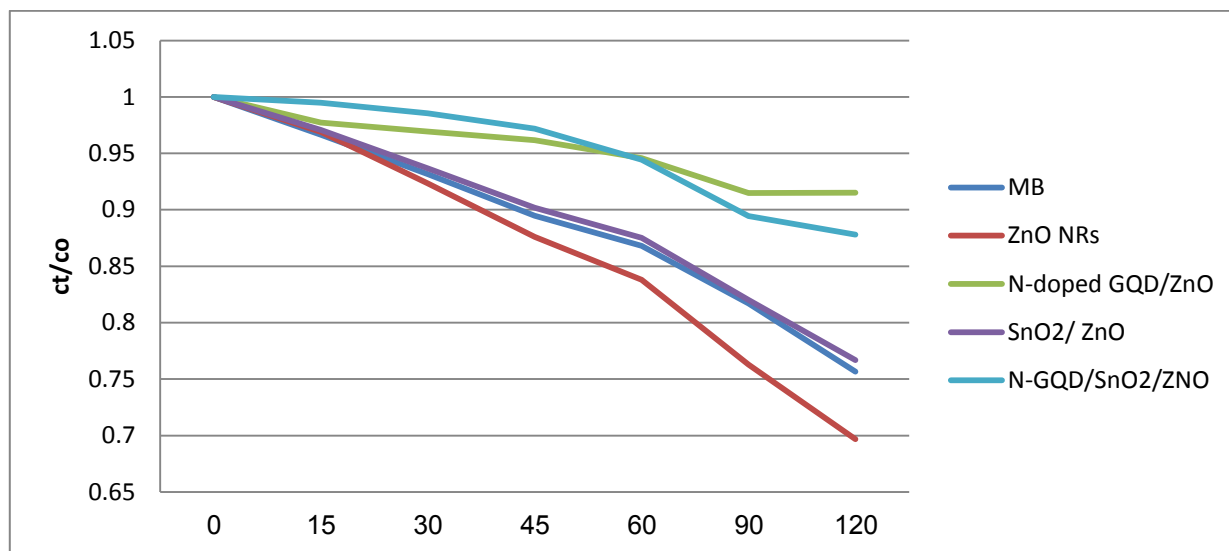
$\ln(C/C_0) = - (ab) t = - k t$, where k is the apparent degradation rate constant.

Figure 25 shows the photocatalytic degradation profile of MB under UV and visible light conditions with ZnO NRs, N-GQDs-U/ ZnO NRs, SnO₂/ZnO NRs composite and N-GQDs-U/ SnO₂/ZnO NRs composite. In figure 25a, the photodegradation of MB by ZnO NRs only was noticed to be the highest, this photodegradation rate was found to be lower using the other substrates. This clearly suggests a direct relationship between visible light photocatalytic activity and surface defect states on ZnO NRs. Typically surface defect states, related to oxygen vacancies, are available to trap electrons or holes. Thus, reducing the probability of recombination of the e-h pairs and subsequent redox reactions may occur. The effectiveness of ZnO NPs in MB decomposition can be explained on the basis of the $\bullet\text{OH}$ radicals and holes present on the surface of ZnO NPs, which break down MB dye in aqueous solutions. In other words, the photocatalytic degradation of the MB is

controlled by the diffusion and reaction of $\text{OH}\cdot$ radicals. However, when ZnO NRs were coated with tin oxide, the rate of these defects decreased; in turn increasing the rate of recombination of electron-hole pairs needed for the photocatalytic reactions. It can be noticed also, that the degradation rate of MB by N-GQDs-U/ZnO NRs substrate was lower than with ZnO NRs substrate, this decrease can be explained by the fact that we synthesize a highly defective graphene quantum dots, in which the generated holes were lost in these big defects and thereby did not react with electron donors species and finally didn't contribute in the photocatalytic activity. The figure 25b shows that the photodegradation rate of MB under visible light conditions using N-GQDs-U/ZnO and N-GQDs-U/ SnO_2 /ZnO NRs composites are the lowest. This decrease in the rate of degradation is due to the wide band gap energy of the prepared N-GQDs-U which is bigger than the controlled by the diffusion and reaction of $\text{OH}\cdot$ radicals. However, when ZnO NRs were coated with tin oxide, the rate of these defects decreased; in turn increasing the rate of recombination of electron-hole pairs needed for the photocatalytic reactions. It can be noticed also, that the degradation rate of MB by N-GQDs-U/ZnO NRs substrate was lower than with ZnO NRs substrate, this decrease can be explained by the fact that we synthesize a highly defective graphene quantum dots, in which the generated holes were lost in these big defects and thereby did not react with electron donors species and finally didn't contribute in the photocatalytic activity. The figure 24b shows that the photodegradation rate of MB under visible light conditions using N-GQDs-U/ZnO and N-GQDs-U/ SnO_2 /ZnO NRs composites are the lowest. This decrease in the rate of degradation is due to the wide band gap energy of the prepared N-GQDs-U which is bigger than the band gap of ZnO NRs. This wide band gap is due to the small sizes of our GQDs, noting that the smaller the size of these GQDs is the bigger is the band gap energy. Therefore, it can be said that our GQDs do not play a separate role in the increased absorption.



(a)



(b)

Figure 25: Time variation of photocatalytic activities of ZnO NRS, N-GQDs-U/ZnO NRs, SnO₂/ZnO NRs composite and N-GQDs-U/SnO₂/ZnO NRs composite under (a) UV light conditions (b) visible light conditions.

Conclusion

The main goal of this project is to highlight the problem of water pollution by microplastics. This report shows the effect of this problem on human being lives and on animals, it also shows some traditional techniques that have been used to clean the water from pollutants. Also, it focused on the photocatalytic degradation technique which gains more and more attention over the years. In this report, we show the different types of semiconductors that can be used as photocatalyst for the photodegradation of pollutants, but we are focusing on zinc oxide semiconductor because of its numerous advantages. In addition, we show the different types of zinc oxide nanomaterials and the technique used for the growing of the ZnO NRs while showing the effect of growing parameters and the ZnO properties on the photocatalytic activity. On the other hand, this report discusses the different ways to improve ZnO NPs as photocatalyst. Among these techniques, we chose to dope our ZnO NRs by graphene quantum dots. Thereby, we designed and synthesized our ZnO NRs first, then we coated them with tin oxide to protect our zinc oxide from photocorrosion and finally, we dipped our substrates in the synthesized N-doped-GQDs. The optical absorption and photoluminescence (PL) spectra of the ZnO NRs, N-GQDs-U, and N-doped GQD-U/ZnO NRs were recorded in a UV/Vis spectrometer and a fluorescence spectrometer. The photocatalytic degradation profile of MB shows that the photodegradation of MB by ZnO NRs was noticed to be the highest, this photodegradation rate was found to be lower using the other substrates. This is explained by the fact that when ZnO NRs were coated with tin oxide, the rate of defects decreased; in turn increases the rate of recombination of electron-hole pairs needed for the photocatalytic reactions. Plus, the decrease in the degradation rate of MB by N-GQDs-U/ZnO NRs composite when compared to ZnO NRs substrate is explained by the fact that we synthesize a highly defective graphene quantum dots, in which the generated holes were lost in these big defects and thereby did not react with electron donors species and finally didn't contribute in the photocatalytic activity. Finally, as a solution to this problem we suggested to anneal our N-GQDs-U/ZnO NRs composite in order to reduce the number of these trap states.

References

- [1] P.R. Gogate, A.B. Pandit, A review of imperative technologies for wastewater treatment I: oxidation technologies at ambient conditions, *Adv. Environ. Res.* 8 (2004) 501e551.
- [2] J. Low, J. Yu, W. Ho, Graphene-based photocatalysts for CO₂ reduction to solar fuel, *J. Phys. Chem. Lett.* 6 (2015) 4244e4251.
- [3] M. Liu, J. Xu, B. Cheng, W. Ho, J. Yu, Synthesis and adsorption performance of Mg(OH)₂ hexagonal nanosheet/graphene oxide composites, *Appl. Surf. Sci.* 332 (2015) 121e129.
- [4] X. Li, J. Yu, M. Jaroniec, Hierarchical photocatalysts, *Chem. Soc. Rev.* 45 (2016) 2603e2636.
- [5] S. Wang, X. Yang, X. Zhang, X. Ding, Z. Yang, K. Dai, H. Chen, A plate-on-plate sandwiched Z-scheme heterojunction photocatalyst: BiOBr-Bi₂MoO₆ with enhanced photocatalytic performance, *Appl. Surf. Sci.* 391 (2017) 194e201.
- [6] Y. Zhang, G. Zhu, M. Hojamberdiev, J. Gao, J. Hao, J. Zhou, P. Liu, Synergistic effect of oxygen vacancy and nitrogen doping on enhancing the photocatalytic activity of Bi₂O₂CO₃ nanosheets with exposed {001} facets for the degradation of organic pollutants, *Appl. Surf. Sci.* 371 (2016) 231e241.
- [7] Y. Guo, S. Lin, X. Li, Y. Liu, Amino acids assisted hydrothermal synthesis of hierarchically structured ZnO with enhanced photocatalytic activities, *Appl. Surf. Sci.* 384 (2016) 83e91.
- [8] S. Duo, Y. Li, Z. Liu, R. Zhong, T. Liu, H. Xu, Preparation of ZnO from 2 D nanosheets to diverse 1 D nanorods and their structure, surface area, photocurrent, optical and photocatalytic properties by simple hydrothermal synthesis, *J. Alloys Compd.* 695 (2017) 2563e2579.
- [9] J. Schneider, M. Matsuoka, M. Takeuchi, J. Zhang, Y. Horiuchi, M. Anpo, D.W. Bahnemann, Understanding TiO₂ photocatalysis: mechanisms and materials, *Chem. Rev.* 114 (2014) 9919e9986.
- [10] K. Qi, F. Zasada, W. Piskorz, P. Indyka, J. Grybo_s, M. Trochowski, M. Buchalska, M. Kobielski, W. Macyk, Z. Sojka, Self-Sensitized photocatalytic degradation of colorless organic pollutants attached to rutile nanorods: experimental and theoretical DFTD studies, *J. Phys. Chem. C* 120 (2016) 5442e5456.
- [11] J. Yu, S. Wang, J. Low, W. Xiao, Enhanced photocatalytic performance of direct Z-scheme g-C₃N₄/TiO₂ photocatalysts for the decomposition of formaldehyde in air, *Phys. Chem. Chem. Phys.* 15 (2013) 16883e16890.
- [12] J. Liu, B. Cheng, J. Yu, A new understanding of the photocatalytic mechanism of the direct Z-scheme g-C₃N₄/TiO₂ heterostructure, *Phys. Chem. Chem. Phys.* (2016) 31175e31183.
- [13] L. Gomathi Devi, R. Kavitha, A review on plasmonic metal-TiO₂ composite for generation, trapping, storing and dynamic vectorial transfer of photogenerated electrons across the Schottky junction in a photocatalytic system, *Appl. Surf. Sci.* 360 (2016) 601e622.
- [14] J. Jin, J. Yu, D. Guo, C. Cui, W. Ho, A hierarchical Z-scheme CdSeWO₃ photocatalyst with enhanced CO₂ reduction activity, *Small* 11 (2015) 5262e5271.
- [15] X. Li, T. Xia, C. Xu, J. Murowchick, X. Chen, Synthesis and photoactivity of nanostructured CdSeTiO₂ composite catalysts, *Catal. Today* 225 (2014) 64e73.
- [16] Y. Hong, J. Zhang, F. Huang, J. Zhang, X. Wang, Z. Wu, Z. Lin, J. Yu, Enhanced visible light photocatalytic hydrogen production activity of CuS/ZnS nanoflower spheres, *J. Mater. Chem. A* 3 (2015) 13913e13919.
- [17] M. Plaza, X. Huang, J.Y.P. Ko, M. Shen, B.H. Simpson, J. Rodríguez-L_opez, N.L. Ritzert, K. Letchworth-Weaver, D. Gunceler, D.G. Schlom, T.A. Arias, J.D. Brock, H.D. Abru~na, Structure of the photo-catalytically active surface of SrTiO₃, *J. Am. Chem. Soc.* 138 (2016) 7816e7819.
- [18] X. Liu, J. Jiang, Y. Jia, J. Qiu, T. Xia, Y. Zhang, Y. Li, X. Chen, Insight into synergistically enhanced adsorption and visible light photocatalytic performance of Z-scheme heterojunction of SrTiO₃(La,Cr)-decorated WO₃ nanosheets, *Appl. Surf. Sci.* 412 (2017) 279e289.
- [19] J. Wen, J. Xie, R. Shen, X. Li, X. Luo, H. Zhang, A. Zhang, G. Bi, Markedly enhanced visible-light photocatalytic H₂ generation over g-C₃N₄ nanosheets decorated by robust nickel phosphide (Ni₁₂P₅) cocatalysts, *Dalton Trans.* 46 (2017) 1794e1802.

- [20] X. Liu, A. Jin, Y. Jia, T. Xia, C. Deng, M. Zhu, C. Chen, X. Chen, Synergy of adsorption and visible-light photocatalytic degradation of methylene blue by a bifunctional Z-scheme heterojunction of WO₃/g-C₃N₄, *Appl. Surf. Sci.* 405 (2017) 359e371.
- [21] J. Wen, J. Xie, Z. Yang, R. Shen, H. Li, X. Luo, X. Chen, X. Li, Fabricating the robust g-C₃N₄ nanosheets/carbons/NiS multiple heterojunctions for enhanced photocatalytic H₂ generation: an insight into the trifunctional roles of nanocarbons, *ACS Sustain. Chem. Eng.* 5 (2017) 2224e2236.
- [22] B. Zhu, P. Xia, Y. Li, W. Ho, J. Yu, Fabrication and photocatalytic activity enhanced mechanism of direct Z-scheme g-C₃N₄/Ag₂WO₄ photocatalyst, *Appl. Surf. Sci.* 391 (2017) 175e183.
- [23] C. Bi, J. Cao, H. Lin, Y. Wang, S. Chen, BiOI/Bi₁₂O₁₇Cl₂: a novel heterojunction composite with outstanding photocatalytic and photoelectric performances, *Mater. Lett.* 166 (2016) 267e270.
- [24] R. He, S. Cao, J. Yu, Recent advances in morphology control and surface modification of Bi-Based photocatalysts, *Acta Phys. Chim. Sin.* 32 (2016) 2841e2870.
- [25] K.M. Lee, C.W. Lai, K.S. Ngai, J.C. Juan, Recent developments of zinc oxide based photocatalyst in water treatment technology: a review, *Water Res.* 88 (2016) 428e448.
- [26] T. Cun, C. Dong, Q. Huang, Ionothermal precipitation of highly dispersive ZnO nanoparticles with improved photocatalytic performance, *Appl. Surf. Sci.* 384 (2016) 73e82.
- [27] K.N. Abbas, N. Bidin, Morphological driven photocatalytic activity of ZnO nanostructures, *Appl. Surf. Sci.* 394 (2017) 498e508.
- [28] M. Khademalrasool, M. Farbod, A. Irajizad, Preparation of ZnO nanoparticles/ Ag nanowires nanocomposites as plasmonic photocatalysts and investigation of the effect of concentration and diameter size of Ag nanowires on their photocatalytic performance, *J. Alloys Compd.* 664 (2016) 707e714.
- [29] M. Gancheva, M. Markova-Velichkova, G. Atanasova, D. Kovacheva, I. Uzunov, R. Cukeva, Design and photocatalytic activity of nanosized zinc oxides, *Appl. Surf. Sci.* 368 (2016) 258e266.
- [30] Z.L. Wang, Nanostructures of zinc oxide, *Mater. Today* 7 (2004) 26e33.
- [31] C. Hariharan, Photocatalytic degradation of organic contaminants in water by ZnO nanoparticles: Revisited, *Appl. Catal. A Gen.* 304 (2006) 55e61.
- [32] A. Akyol, H.C. Yatmaz, M. Bayramoglu, Photocatalytic decolorization of remazol red RR in aqueous ZnO suspensions, *Appl. Catal. B Environ.* 54 (2004) 19e24.
- [33] G. Colón, M.C. Hidalgo, J.A. Navío, E. Pulido Melián, O. González Díaz, J.M. Domínguez Rodríguez, Highly photoactive ZnO by amine capping-assisted hydrothermal treatment, *Appl. Catal. B Environ.* 83 (2008) 30e38.
- [34] C. Lizama, J. Freer, J. Baeza, H.D. Mansilla, Optimized photodegradation of reactive blue 19 on TiO₂ and ZnO suspensions, *Catal. Today* 76 (2002) 235e246.
- [35] D. Mijin, M. Savić, P. Snežana, A. Smiljanić, O. Glavaški, M. Jovanović, S. Petrović, A study of the photocatalytic degradation of metamitron in ZnO water suspensions, *Desalination* 249 (2009) 286e292.
- [36] S. Ambika, M. Sundrarajan, Antibacterial behaviour of Vitex negundo extract assisted ZnO nanoparticles against pathogenic bacteria, *J. Photochem. Photobiol. B* 146 (2015) 52e57.
- [37] J. Panigrahi, D. Behera, I. Mohanty, U. Subudhi, B.B. Nayak, B.S. Acharya, Radio frequency plasma enhanced chemical vapor based ZnO thin film deposition on glass substrate: a novel approach towards antibacterial agent, *Appl. Surf. Sci.* 258 (2011) 304e311.
- [38] P. Zhu, Z. Weng, X. Li, X. Liu, S. Wu, K.W.K. Yeung, X. Wang, Z. Cui, X. Yang, P.K. Chu, Biomedical applications of functionalized ZnO nanomaterials: from biosensors to bioimaging, *Adv. Mater. Interfaces* 3 (2016) 1500494.
- [39] V. Svetlichnyi, A. Shabalina, I. Lapin, D. Goncharova, A. Nemoykina, ZnO nanoparticles obtained by pulsed laser ablation and their composite with cotton fabric: preparation and study of antibacterial activity, *Appl. Surf. Sci.* 372 (2016) 20e29.
- [40] S. George, S. Pokhrel, T. Xia, B. Gilbert, Z. Ji, M. Schowalter, A. Rosenauer, R. Damoiseaux, K.A. Bradley, L. McAdler, A.E. Nel, Use of a rapid cytotoxicity screening approach to engineer a safer zinc oxide nanoparticle through iron doping, *ACS Nano* 4 (2010) 15e29.
- [41] V. Kononenko, N. Repar, N. Marušić, B. Drašler, T. Romih, S. Hočevar, D. Drobne, Comparative in vitro genotoxicity study of ZnO nanoparticles, ZnO macroparticles and ZnCl₂ to MDCK kidney cells: size matters, *Toxicol. in Vitro* 40 (2017) 256e263.

- [42] S. Hackenberg, A. Scherzed, A. Technau, M. Kessler, K. Froelich, C. Ginzkey, C. Koehler, M. Burghartz, R. Hagen, N. Kleinsasser, Cytotoxic, genotoxic and pro-inflammatory effects of zinc oxide nanoparticles in human nasal mucosa cells in vitro, *Toxicol. in Vitro* 25 (2011) 657e663.
- [43] V. Kandavelu, H. Kastien, K.R. Thampi, Photocatalytic degradation of isothiazolin-3-ones in water and emulsion paints containing nanocrystalline TiO₂ and ZnO catalysts, *Appl. Catal. B Environ.* 48 (2004) 101e111.
- [44] M.D. Hernandez-Alonso, F. Fresno, S. Suarez, J.M. Coronado, Development of alternative photocatalysts to TiO₂: challenges and opportunities, *Energy Environ. Sci.* 2 (2009) 1231e1257.
- [45] R. Shi, P. Yang, X. Song, J. Wang, Q. Che, A. Zhang, ZnO flower: self-assembly growth from nanosheets with exposed {1-100} facet, white emission, and enhanced photocatalysis, *Appl. Surf. Sci.* 366 (2016) 506e513.
- [46] S.-W. Zhao, H.-F. Zuo, Y.-R. Guo, Q.-J. Pan, Carbon-doped ZnO aided by carboxymethyl cellulose: fabrication, photoluminescence and photocatalytic applications, *J. Alloys Compd.* 695 (2017) 1029e1037.
- [47] R. Rooydell, S. Brahma, R.-C. Wang, M.R. Modaberi, F. Ebrahimpzadeh, C.- P. Liu, Cu doped ZnO nanorods with controllable Cu content by using single metal organic precursors and their photocatalytic and luminescence properties, *J. Alloys Compd.* 691 (2017) 936e945.
- [48] R. Nasser, W.B.H. Othmen, H. Elhouichet, M. Ferid, Preparation, characterization of Sb-doped ZnO nanocrystals and their excellent solar light driven photocatalytic activity, *Appl. Surf. Sci.* 393 (2017) 486e495.
- [49] O. Altintas Yildirim, H. Arslan, S. Sonmezoglu, Facile synthesis of cobaltdoped zinc oxide thin films for highly efficient visible light photocatalysts, *Appl. Surf. Sci.* 390 (2016) 111e121.
- [50] S.A. Ansari, M.M. Khan, M.O. Ansari, J. Lee, M.H. Cho, Biogenic synthesis, photocatalytic, and photoelectrochemical performance of Ag/ZnO nanocomposite, *J. Phys. Chem. C* 117 (2013) 27023e27030.
- [51] N. Güy, M. Özacar, The influence of noble metals on photocatalytic activity of ZnO for Congo red degradation, *Int. J. Hydrogen Energy* 41 (2016) 20100e20112.
- [52] V.E. Podasca, T. Buruiana, E.C. Buruiana, UV-cured polymeric films containing ZnO and silver nanoparticles with UV-vis light-assisted photocatalytic activity, *Appl. Surf. Sci.* 377 (2016) 262e273.
- [53] S. Sohrabnezhad, A. Seifi, The green synthesis of Ag/ZnO in montmorillonite with enhanced photocatalytic activity, *Appl. Surf. Sci.* 386 (2016) 33e40.
- [54] J. Low, J. Yu, M. Jaroniec, S. Wageh, A.A. Al-Ghamdi, Heterojunction photocatalysts, *Adv. Mater.* 29 (2017) 1601694.
- [55] Y.-C. Chang, Complex ZnO/ZnS nanocable and nanotube arrays with high performance photocatalytic activity, *J. Alloys Compd.* 664 (2016) 538e546.
- [56] X. Liu, Q. Lu, J. Liu, Electrospinning preparation of one-dimensional ZnO/ Bi₂WO₆ heterostructured sub-microbelts with excellent photocatalytic performance, *J. Alloys Compd.* 662 (2016) 598e606.
- [57] S. Thangavel, S. Thangavel, N. Raghavan, K. Krishnamoorthy, G. Venugopal, Visible-light driven photocatalytic degradation of methylene-violet by rGO/ Fe₃O₄/ZnO ternary nanohybrid structures, *J. Alloys Compd.* 665 (2016) 107e112.
- [58] J. Tao, Z. Gong, G. Yao, Y. Cheng, M. Zhang, J. Lv, S. Shi, G. He, X. Jiang, X. Chen, Z. Sun, Enhanced optical and photocatalytic properties of Ag quantum dotssensitized nanostructured TiO₂/ZnO heterojunctions, *J. Alloys Compd.* 688 (2016) 605e612.
- [59] M. Samadi, H.A. Shivaee, M. Zanetti, A. Pourjavadi, A. Moshfegh, Visible light photocatalytic activity of novel MWCNT-doped ZnO electrospun nanofibers, *J. Mol. Catal. A Chem.* 359 (2012) 42e48.
- [60] T. Xu, L. Zhang, H. Cheng, Y. Zhu, Significantly enhanced photocatalytic performance of ZnO via graphene hybridization and the mechanism study, *Appl. Catal. B Environ.* 101 (2011) 382e387.
- [61] H. Fu, T. Xu, S. Zhu, Y. Zhu, Photocorrosion inhibition and enhancement of photocatalytic activity for ZnO via hybridization with C₆₀, *Environ. Sci. Technol.* 42 (2008) 8064e8069.
- [62] T. Chen, S. Yu, X. Fang, H. Huang, L. Li, X. Wang, H. Wang, Enhanced photocatalytic activity of C@ZnO core-shell nanostructures and its photoluminescence property, *Appl. Surf. Sci.* 389 (2016) 303e310.
- [63] M. Yu, Y. Ma, J. Liu, X. Li, S. Li, S. Liu, Sub-coherent growth of ZnO nanorod arrays on three-dimensional graphene framework as one-bulk high-performance photocatalyst, *Appl. Surf. Sci.* 390 (2016) 266e272.

- [64] S. Bera, M. Pal, A. Naskar, S. Jana, Hierarchically structured ZnO-graphene hollow microspheres towards effective reusable adsorbent for organic pollutant via photodegradation process, *J. Alloys Compd.* 669 (2016) 177e186.
- [65] PlasticsEurope, Plastics – the Facts 2014/2015-An analysis of European plastics production, demand and waste data, <http://www.plasticseurope.org/Document/plastics-the-facts-20142015.aspx?Page¼DOCUMENT&FolID¼42>, 2015.
- [66] D. K. A. Barnes, F. Galgani, R. C. Thompson and M. Barlaz, *Philos. Trans. R. Soc., B*, 2009, 364, 1985–1998.
- [67] I. Roy and P. M. Visakh, Polyhydroxyalkanoate (PHA) based blends, composites and nanocomposites, Royal Society of Chemistry, Cambridge, U.K., 2015.
- [68] T. N. Hofer, *Marine Pollution: New Research*, Nova Science Publishers, New York, 2008.
- [69] Sharma S, Chatterjee S. Microplastic pollution, a threat to marine ecosystem and human health: a short review. *Environ Sci Pollut Res.* 2017;24:21530–47.
- [70] Auta HS, Emenike C, Fauziah SH. Distribution and importance of microplastics in the marine environment: a review of the sources, fate, effects and potential solutions. *Environ Int.* 2017;102:165–76.
- [71] PlasticsEurope, Plastics – the Facts 2012 An analysis of European plastics production, demand and waste data for 2011, http://www.plasticseurope.org/documents/document/20121120170458nal_plasticsthefacts_nov2012_en_web_resolution.pdf, 2012.
- [72] J. Murphy, *Additives for plastics handbooks*, Elsevier Science Ltd, Kidlington, Oxford, UK, New York, NY, USA, 2nd edn, 2001.
- [73] *Plastics Additives*, ed. G. Pritchard, Springer, Netherlands, Dordrecht, 1998, vol. 1.
- [74] Stringer and P. Johnston, *Environ. Sci. Pollut. Res.*, 2001, 8, 146.
- [75] Park Y, Lee S, Kang SO, Choi W (2010) Organic dye-sensitized TiO₂ for the redox conversion of water pollutants under visible light. *Chemical Communications* 46(14): 2477-2479.
- [76] Hoffmann MR, Martin ST, Choi W, Bahnemann DW (1995) Environmental applications of semiconductor photocatalysis. *Chemical Reviews* 95(1): 69-9
- [77] Linsebigler AL, Lu GQ, Yates JT (1995) Photocatalysis on TiO₂ surfaces: principles, mechanisms and selected results. *Chem Rev* 95(3): 735-758.
- [78] Stewart G, Fox MA (1995). The effect of dark recovery time on the photoefficiency of heterogeneous photocatalysis by TiO₂ suspended in non-aqueous media. *Res Chem Intermediates* 21: 933-938.
- [79] Prata J. Airborne microplastics: consequences to human health? *Environ Pollut.* 2018;234:115–26.
- [80] Brien, S., 2007. Vinyls Industry Update. Presentation at the World Vinyl Forum 2007, Sept. 2007. Retrieved from <http://vinyl-institute.com/Publication/WorldVinylForumIII/VinylIndustryUpdate.aspx>.
- [81] Li X, Liu G, Zhao J (1999) Two competitive primary processes in the photodegradation of cationic triaryl methane dyes under visible irradiation in TiO₂ dispersions. *New J Chem* 23: 1193-1196.
- [82] Deng F, Li Y, Luo X, Yang L, Tu X, et al. (2012) Preparation of conductive polypyrrole/TiO₂ nanocomposite via surface molecular imprinting technique and its photocatalytic activity under simulated solar light irradiation. *Colloids and Surfaces A: Physicochem Eng Aspects* 395: 183-189.
- [83] Chen CC, Lu CS (2007) Photocatalytic degradation of Basic Violet 4: degradation efficiency, product distribution, and mechanisms. *J Phys Chem C* 111(37): 13922-13932.
- [84] Plumlee MH, Larabee J, Reinhard M. Perfluorochemicals in water reuse. *Chemosphere* 2008; 72:1541–7. <http://dx.doi.org/10.1016/j.chemosphere.2008.04.057>.
- [85] Serpone N (1994) A decade of heterogeneous photocatalysis in our laboratory: pure and applied studies in energy production and environmental detoxification. *Research on Chemical Intermediates* 20(9): 953-992.
- [86] Zamaraev KI, Khramov MI, Parmon VN (1994) Possible impact of heterogeneous photocatalysis on the global chemistry of the earth's atmosphere. *Cat Rev Sci Eng* 36(4): 617-644.
- [87] Kamat PV (1993) Photochemistry on nonreactive and reactive (semiconductor) surfaces. *Chem Rev* 93(1): 267-300.
- [88] Liang HC, Li XZ (2009) Visible-induced photocatalytic reactivity of polymer-sensitized titania nanotube films. *Applied Catalysis B: Environmental* 86(1-2): 8-17.

- [89] Ferreira C, Domenech S, Lacaze P (2001) Synthesis and characterization of polypyrrole/TiO₂ composites on mild steel. *J of Applied Electrochemistry* 31(1): 49-56.
- [90] Saquib M, Muneer M (2003) TiO₂-mediated photocatalytic degradation of a triphenylmethane dye (gentian violet), in aqueous suspensions. *Dyes Pigments* 56(1): 37-49.
- [91] USEPA, *Handbook Advanced Photochemical Oxidation Processes*, Office of Research and Development, Washington, DC, USA, 1998, EPA/625/R-98/004.
- [92] P. Le-Clech, E. K. Lee, and V. Chen, "Hybrid photocatalysis/ membrane treatment for surface waters containing low concentrations of natural organic matters," *Water Research*, vol. 40, no. 2, pp. 323–330, 2006.
- [93] Guo, Z., B. Sa, B. Pathak, J. Zhou, R. Ahuja, and Z. Sun. 2014. Band gap engineering in huge-gap semiconductor SrZrO₃ for visible light photocatalysis. *Int. J. Hydrogen Energy*. 39(5): 2042-2048.
- [94] Miseki, Y., O. Kitao, and K. Sayama. 2015. Photocatalytic water oxidation over PbCrO₄ with 2.3 eV band gap in IO₃⁻/I⁻ redox mediator under visible light. *RSC Adv.* 5(2): 1452-1455.
- [95] Chen, O. J, J. Chen, T. Wang, Z. Li, and X. Dou. 2015. The photovoltaic properties of novel narrow band gaps Cu₂SnS₃ films prepared by spray pyrolysis method. *RSC Adv.* 5(37): 28885-28891.
- [96] Kumawat, P., M. Joshi, R. Ameta, and S. C. Ameta. 2015. Photocatalytic degradation of basic fuchism over quaternary oxide iron zinc cuprate (FeZn₂Cu₃O_{6.5}). *Adv. Appl. Sci. Res.* 6(7): 209-215.
- [97] Luan, J., W. Zhao, J. Feng, H. Cai, Z. Zheng, B. Pan, X. Wu, Z. Zou, and Y. Li. 2009. Structural, photophysical and photocatalytic properties of novel Bi₂AlVO₇. *J. Hazard. Mater.* 164(2-3): 781-789.
- [98] Reshak, A. H., K. Nouneh, I. V. Kityk, J. BILA, S. Auluck, H. Kamarudin, and Z. Sekkat. 2014. Structural, electronic and optical properties in earth-abundant.
- [99] Yu, B., K. M. Leung, Q. Guo, W. M. Lau, and J. Yang. 2011. Synthesis of Ag-TiO₂ composite nano thin film for antimicrobial application, *Nanotechnology*. 22(11): 115603.
- [100] Sekiguchi, Y., Y. Yao, Y. Ohko, K. Tanaka, T. Ishido, A. Fujishima, and Y. Kubota. 2007. Self-sterilizing catheters with titanium dioxide photocatalyst thin films for clean intermittent catheterization: Basics and study of clinical use. *Int. J. Urol.* 14(5): 426-430.
- [101] Nakamura, H., M. Tanaka, S. Shinohara, M. Gotoh, and I. Karube. 2007. Development of a self-sterilizing lancet coated with a titanium dioxide photocatalytic nano-layer for self-monitoring of blood glucose. *Biosens. Bioelectron.* 22(9- 10): 1920-1925.
- [102] Su, J., L. Guo, N. Bao, and C. A. Grimes. 2011. Nanostructured WO₃/BiVO₄ heterojunction films for efficient photoelectrochemical water splitting. *Nano Lett.* 11(5): 1928- 1933.
- [103] Yang, G., Yan, Q. Zhang, S. Shen, and S. Ding. 2013. One dimensional CdS/ZnO core/shell nanofibers via single-spinneret electrospinning: Tunable morphology and efficient photocatalytic hydrogen production. *Nanoscale.* 5(24): 12432- 12439.
- [104] Reddy, P. A. K., G. Srinivas, V. D. Kumari, M. V. Shankar, M. Subrahmanyam, and J.S. Lee. 2014. CaFe₂O₄ sensitized hierarchical TiO₂ photo composite for hydrogen production under solar light irradiation. *Chem. Eng. J.* 247: 152- 160.
- [105] F. Akbal and A. N. Onar, "Photocatalytic degradation of phenol," *Environmental Monitoring and Assessment*, vol. 83, no. 3, pp. 295–302, 2003.
- [106] K. H. Lanouette, "Treatment of phenolic wastes," *Chemical Engineering*, vol. 17, pp. 99–106, 1997.
- [107] N. Singh and J. Singh, "An enzymatic method for removal of phenol from industrial effluent," *Preparative Biochemistry and Biotechnology*, vol. 32, no. 2, pp. 127–133, 2002.
- [108] Guo JF, Ma B, Yin A, Fan K, Dai WL. Highly stable and efficient Ag/AgCl@TiO₂ photocatalyst: preparation, characterization, and application in the treatment of aqueous hazardous pollutants. *J Hazard Mater* 2012;211-212:77-82
- [109] Gratzel M. Photoelectrochemical cells. *Nature* 2001;414:338-44.
- [110] Herrmann J-M. Heterogeneous photocatalysis: fundamentals and applications to the removal of various types of aqueous pollutants. *Catal Today* 1999; 53:115–29. [http://dx.doi.org/10.1016/S0920-5861\(99\)00107-8](http://dx.doi.org/10.1016/S0920-5861(99)00107-8).
- [111] Rajamanickam D, Shanthi M. Photocatalytic degradation of an organic pollutant by zinc oxide – solar process. *Arab J Chem* 2016; 9:S1858–S1868. <http://dx.doi.org/10.1016/j.arabjc.2012.05.006>.

- [112] Rauf MA, Ashraf SS. Fundamental principles and application of heterogeneous photocatalytic degradation of dyes in solution. *Chem Eng J* 2009; 151:10–8. <http://dx.doi.org/10.1016/j.cej.2009.02.026>.
- [113] M. Yu, Y. Ma, J. Liu, X. Li, S. Li, S. Liu, Sub-coherent growth of ZnO nanorod arrays on three-dimensional graphene framework as one-bulk high-performance photocatalyst, *Appl. Surf. Sci.* 390 (2016) 266e272.
- [114] S. Bera, M. Pal, A. Naskar, S. Jana, Hierarchically structured ZnO-graphene hollow microspheres towards effective reusable adsorbent for organic pollutant via photodegradation process, *J. Alloys Compd.* 669 (2016) 177e186.
- [115] R. Ullah, J. Dutta, photocatalytic degradation of organic dyes with manganese-doped ZnO nanoparticles, *J. Hazard. Mater.* 156 (2008) 194-200.
- [116] N.N. Lichtin, M. Avudaithai, E. Berman, A. Grayfer, TiO₂-photocatalyzed oxidative degradation of binary mixtures of vaporized organic compounds, *Sol. Energy* 56 (1996) 377-385.
- [117] D.S. Bhatkhande, V.G. Pangarkar, A.A.C.M. Beenackers, photocatalytic degradation degradation for environmental applications – a review, *J. Chem. Technol. Biotechnol.* 77 (2001) 102- 116.
- [118] A.M. Al-Hamdi, M. Sillanpää, J. Dutta, Photocatalytic degradation of phenol by iodine doped tin oxide nanoparticles under UV and sunlight irradiation, *J. Alloys compd.* 618 (2015) 366- 371.
- [119] S. Baruah, J. Dutta, Hydrothermal growth of ZnO nanostructures, *Sci. Technol. Adv. Mater.* 10 (2009) 013001.
- [120] H. Wahab, A. Salama, A. El Saeid, M. Willander, O. Nur, I. Battisham Zinc oxide nano-rods based glucose biosensor devices fabrication, *Results Phys.* 9 (2018) 809-814.
- [121] Liang S, Xiao K, Mo Y, Huang X. A novel ZnO nanoparticle blended polyvinylidene fluoride membrane for anti-irreversible fouling. *J Memb Sci* 2012; 394:184–92. <http://dx.doi.org/10.1016/j.memsci.2011.12.040>.
- [122] Jang ES, Won J-H, Hwang S-J, Choy J-H. Fine tuning of the face orientation of ZnO crystals to optimize their photocatalytic activity. *Adv Mater* 2006; 18:3309–12. <http://dx.doi.org/10.1002/adma.200601455>.
- [123] Cha SI, Hwang KH, Kim YH, et al. Crystal splitting and enhanced photocatalytic behavior of TiO₂ rutile nano-belts induced by dislocations. *Nanoscale* 2013, 5: 753–758. [124] Baruah, S., Mahmood, M. A., Myint, M. T. Z., Bora, T., & Dutta, J. (2010). Enhanced visible light photocatalysis through fast crystallization of zinc oxide nanorods. *Beilstein Journal of Nanotechnology*, 1, 14–20. <http://doi.org/10.3762/bjnano.1.3>.
- [125] Zhang Y, Ram MK, Stefanakos EK, Goswami DY. Synthesis, characterization, and applications of ZnO nanowires. *J Nanomater* 2012; 2012:1–22. <http://dx.doi.org/10.1155/2012/624520>.
- [126] Banerjee P, Chakrabarti S, Maitra S, Dutta BK. Zinc oxide nano-particles –sonochemical synthesis, characterization and application for photo-remediation heavy metal. *Ultrason Sonochem* 2012; 19:85–93. <http://dx.doi.org/10.1016/j.ultsonch.2011.05.007>.
- [127] Wang F, Qin X, Guo Z, Meng Y, Yang L, Ming Y. Hydrothermal synthesis of dumbbell-shaped ZnO microstructures. *Ceram Int* 2013; 39:8969–73. <http://dx.doi.org/10.1016/j.ceramint.2013.04.096>.
- [128] Fang Y, Li Z, Xu S, Han D, Lu D. Optical properties and photocatalytic activities of spherical ZnO and flower-like ZnO structures synthesized by facile hydrothermal method. *J Alloy Compd* 2013; 575:359–63. <http://dx.doi.org/10.1016/j.jallcom.2013.05.183>.
- [129] Chandrasekaran P, Viruthagiri G, Srinivasan N. The effect of various capping agents on the surface modifications of sol–gel synthesised ZnO nanoparticles. *J Alloy Compd* 2012; 540:89–93. <http://dx.doi.org/10.1016/j.jallcom.2012.06.032>.
- [130] Lim SK, Hwang S-H, Kim S, Park H. Preparation of ZnO nanorods by microemulsion synthesis and their application as a CO gas sensor. *Sens Actuators B Chem* 2011; 160:94–8. <http://dx.doi.org/10.1016/j.snb.2011.07.018>.
- [131] Wan L, Yan S, Feng J, Yang Z, Fan X, Li Z, et al. Solvothermal synthesis of core–shell ZnO hollow microhemispheres. *Colloids Surf A Physicochem Eng Asp* 2012; 396:46–50. <http://dx.doi.org/10.1016/j.colsurfa.2011.12.039>.

- [132] Jiao S, Zhang K, Bai S, Li H, Gao S, Li H, et al. Controlled morphology evolution of ZnO nanostructures in the electrochemical deposition: from the point of view of chloride ions. *Electrochim Acta* 2013; 111:64–70. <http://dx.doi.org/10.1016/j.electacta.2013.08.050>.
- [133] Yue S, Lu J, Zhang J. Controlled growth of well-aligned hierarchical ZnO arrays by a wet chemical method. *Mater Lett* 2009; 63. <http://dx.doi.org/10.1016/j.matlet.2009.06.055>.
- [134] Ushio M, Sumiyoshi Y. Synthesis of ZnO single crystals by the flux method. *J Mater Sci* 1993; 28:218–24. <http://dx.doi.org/10.1007/BF00349054>.
- [135] Wu H, Pan W. Preparation of zinc oxide nanofibers by electrospinning. *J Am Ceram Soc* 2006; 89:699–701. <http://dx.doi.org/10.1111/j.1551-2916.2005.00735.x>.
- [136] Hasanpoor M, Aliofkhazraei M, Delavari H. Microwave-assisted synthesis of zinc oxide nanoparticles. *Procedia Mater Sci* 2015; 11:320–5. <http://dx.doi.org/10.1016/j.mspro.2015.11.101>.
- [137] Lee S, Jeong S, Kim D, Hwang S, Jeon M, Moon J. ZnO nanoparticles with controlled shapes and sizes prepared using a simple polyol synthesis. *Superlattices Microstruct* 2008;43:330–9. <http://dx.doi.org/10.1016/j.spmi.2008.01.004>.
- [138] Vafaei M, Ghamsari MS. Preparation and characterization of ZnO nanoparticles by a novel sol–gel route. *Mater Lett* 2007;61. <http://dx.doi.org/10.1016/j.matlet.2006.11.089>.
- [139] Köse H, Karaal Ş, Aydın AO, Akbulut H. A facile synthesis of zinc oxide/ multiwalled carbon nanotube nanocomposite lithium ion battery anodes by sol–gel method. *J Power Sources* 2015;295:235–45. <http://dx.doi.org/10.1016/j.jpowsour.2015.06.135>.
- [140] Jiang DY, Zhao JX, Zhao M, Liang QC, Gao S, Qin JM, et al. Optical waveguide based on ZnO nanowires prepared by a thermal evaporation process. *J Alloy Compd* 2012;532:31–3. <http://dx.doi.org/10.1016/j.jallcom.2012.03.114>.
- [141] Ma X, Zhang J, Lu J, Ye Z. Room temperature growth and properties of ZnO films by pulsed laser deposition. *Appl Surf Sci* 2010;257:1310–3. <http://dx.doi.org/10.1016/j.apsusc.2010.08.057>.
- [142] Zhang N, Yi R, Shi R, Gao G, Chen G, Liu X. Novel rose-like ZnO nanoflowers synthesized by chemical vapor deposition. *Mater Lett* 2009; 63.<http://dx.doi.org/10.1016/j.matlet.2008.11.046>.
- [143] Ouyang W, Zhu J. Catalyst-free synthesis of macro-scale ZnO nanonail arrays on Si substrate by simple physical vapor deposition. *Mater Lett* 2008;62. <http://dx.doi.org/10.1016/j.matlet.2007.12.051>.
- [144] Lee C-H, Kim D-W. Thickness dependence of microstructure and properties of ZnO thin films deposited by metal-organic chemical vapor deposition using ultrasonic nebulization. *Thin Solid Films* 2013;546:38–41. <http://dx.doi.org/10.1016/j.tsf.2013.05.029>.
- [145] Hu P, Han N, Zhang D, Ho JC, Chen Y. Highly formaldehyde-sensitive, transitionmetal doped ZnO nanorods prepared by plasma-enhanced chemical vapor deposition. *Sens Actuators B Chem* 2012; 169: 74–80. <http://dx.doi.org/10.1016/j.snb.2012.03.035>.
- [146] Wang C, Chen Z, Hu H, Zhang D. Effect of the oxygen pressure on the microstructure and optical properties of ZnO films prepared by laser molecular beam epitaxy. *Phys B Condens Matter* 2009; 404: 4075–82. <http://dx.doi.org/10.1016/j.physb.2009.07.165>.
- [147] Baruah S, Thanachayanont C, Dutta J (2008) *Sci Technol Adv Mater* 9:025009. doi:10.1088/1468-6996/9/2/025009.
- [148] Wei M, Zhi D, MacManus-Driscoll JL (2005) *Nanotechnology* 16:1364. doi:10.1088/0957-4484/16/8/064.
- [149] Paraguay FD, Estrada WL, Acosta DRN, Andrade E, Miki-Yoshida M (1999) *Thin Solid Films* 350:192. doi: 10.1016/S0040-6090(99)00050-4.
- [150] Wang, S.F., Tseng, T.Y., Wang, Y.R., Wang, C.Y., Lu, H.C. and Shih, W.L. (2008) ‘Effects of preparation conditions on the growth of ZnO nanorod arrays using aqueous solution method’, *International Journal of Applied Ceramic Technology*, Vol. 5, No. 5, pp.419–429.
- [151] Xu, S., Lao, C., Weintraub, B. and Wang, Z.L. (2008) ‘Density-controlled growth of aligned ZnO nanowire arrays by seedles chemical approach on smooth surfaces’, *Journal of Materials Research*, Vol. 23, No. 8, pp.2072–2077.
- [152] Zhou, Z., Zhao, Y. and Cai, Z. (2010) ‘Low-temperature growth of ZnO nanorods on PET fabrics with two-step hydrothermal method’, *Applied Surface Science*, Vol. 256, No. 14, pp.4724–4728.

- [153] Dutta, P.K., Pehkonen, S.O., Sharma, V.K. and Ray, A.K. (2005) 'Photocatalytic oxidation of arsenic (III): evidence of hydroxyl radicals', *Environmental Science and Technology*, Vol. 39, No. 6, pp.1827–1834.
- [154] P. Erhart, K. Albe, *Appl. Phys. Lett.* 88 (2006) 201918.
- [155] X.Q. Wei, Z.G. Zhang, M. Liu, C.S. Chen, G. Sun, C.S. Xue, H.Z. Zhuang, B.Y. Man, *Mater. Chem. Phys.* 101 (2007) 285–290.
- [156] S. Baruah, M.A. Mahmood, M.T.Z. Myint, T. Bora, J. Dutta, *Beilstein J. Nanotechnol.* 1 (2010) 14–20.
- [157] Y. Peng, Y. Wang, Q.-G. Chen, Q. Zhu, A.W. Xu, *CrystEngComm* 16 (2014) 7906–7913.
- [158] R.M. Sheetz, I. Ponomareva, E. Richter, A.N. Andriotis, M. Menon, *Phys. Rev. B* 80 (2009) 195314.
- [159] X. Zhang, J. Qin, Y. Xue, P. Yu, B. Zhang, L. Wang, R. Liu, *Sci. Rep.* 4 (2014) 4596.
- [160] S.R.A. Raza, Y.T. Lee, Y.-G. Chang, P.J. Jeon, J.H. Kim, R. Ha, H.-J. Choi, S. Im, *Phys. Chem. Chem. Phys.* 15 (2013) 2660–2664.
- [161] S. Baruah, S.S. Sinha, B. Ghosh, S.K. Pal, A.K. Raychaudhuri, J. Dutta, *J. Appl. Phys.* 105 (2009) 074308.
- [162] S. Baruah, S.S. Sinha, B. Ghosh, S.K. Pal, A.K. Raychaudhuri, J. Dutta, *J. Appl. Phys.* 105 (2009) 074308.
- [163] M.K. Kavitha, K.B. Jinesh, R. Philip, P. Gopinath, H. John, *Phys. Chem. Chem. Phys.* 16 (2014) 25093–25100.
- [164] P. Attri, Y.H. Kim, D.H. Park, J.H. Park, Y.J. Hong, H.S. Uhm, K.-N. Kim, A. Fridman, E.H. Choi, *Sci. Rep.* 5 (2015) 9332.
- [165] S.G. Kumar, K.S.R.K. Rao, *RSC Adv.* 5 (2015) 3306–3351.
- [166] C.G. Van de Walle, *Phys. B* 308–310 (2001) 899–903.
- [167] S. Akir, A. Barras, Y. Coffinier, M. Bououdina, R. Boukherroub, A.D. Omrani, *Ceram. Int.* 42 (2016) 10259–10265.
- [168] K.M. Lee, C.W. Lai, K.S. Ngai, J.C. Juan, *Water Res.* 88 (2016) 428–448.
- [169] O. Fumiyasu, C. Minseok, T. Atsushi, T. Isao, *Sci. Technol. Adv. Mater.* 12 (2011) 034302–034315.
- [170] A. Janotti, C.G. Van de Walle, *J. Cryst. Growth* 287 (2006) 58–65.
- [171] A. Janotti, C.G. Van De Walle, *Phys. Rev. B* 76 (2007) 165202–165224.
- [172] Guo, M. Y. et al. Effect of Native Defects on Photocatalytic Properties of ZnO. *J. Phys. Chem. C* 115, 11095–11101 (2011).
- [173] Wang, J.-L., Wang, J.-Q., He, L.-N., Dou, X.-Y. & Wu, F. A CO₂/H₂O₂-tunable reaction: direct conversion of styrene into styrene carbonate catalyzed by sodium phosphotungstate/n-Bu₄NBr. *Green Chem.* 10, 1218–1223 (2008).
- [174] Zheng, Y. et al. Luminescence and Photocatalytic Activity of ZnO Nanocrystals: Correlation between Structure and Property. *Inorg. Chem.* 46, 6675–6682 (2007).
- [175] Kong, M. et al. Tuning the Relative Concentration Ratio of Bulk Defects to Surface Defects in TiO₂ Nanocrystals Leads to High Photocatalytic Efficiency. *J. Am. Chem. Soc.* 133, 16414–16417 (2011).
- [176] Jang, E. S., Won, J. H., Hwang, S. J. & Choy, J. H. Fine Tuning of the Face Orientation of ZnO Crystals to Optimize Their Photocatalytic Activity. *Adv. Mater.* 18, 3309–3312 (2006).
- [177] McLaren, A., Valdes-Solis, T., Li, G. & Tsang, S. C. Shape and Size Effects of ZnO Nanocrystals on Photocatalytic Activity. *J. Am. Chem. Soc.* 131, 12540–12541 (2009).
- [178] C. Han, M.-Q. Yang, B. Weng, Y.-J. Xu, Improving the photocatalytic activity and anti photocorrosion of semiconductor ZnO by coupling with versatile carbon, *Phys. Chem. Chem. Phys.* 16 (2014) 16891e16903.
- [179] P. Senthil Kumar, M. Selvakumar, S. Ganesh Babu, S. Induja, S. Karuthapandian, CuO/ZnO nanorods: an affordable efficient p-n heterojunction and morphology dependent photocatalytic activity against organic contaminants, *J. Alloys Compd.* 701 (2017) 562e573.
- [180] W. Kang, X. Jimeng, W. Xitao, The effects of ZnO morphology on photocatalytic efficiency of ZnO/RGO nanocomposites, *Appl. Surf. Sci.* 360 (2016) 270e275.
- [181] Y. Liu, R. Wang, Z. Yang, H. Du, Y. Jiang, C. Shen, K. Liang, A. Xu, Enhanced visible-light photocatalytic activity of Z-scheme graphitic carbon nitride/ oxygen vacancy-rich zinc oxide hybrid photocatalysts, *Chin. J. Catal.* 36 (2015) 2135e2144.
- [182] J. Yu, X. Yu, Hydrothermal synthesis and photocatalytic activity of zinc oxide hollow spheres, *Environ. Sci. Technol.* 42 (2008) 4902e4907.

- [183] L. Pan, G.-Q. Shen, J.-W. Zhang, X.-C. Wei, L. Wang, J.-J. Zou, X. Zhang, TiO₂/ZnO composite sphere decorated with ZnO clusters for effective charge isolation in photocatalysis, *Ind. Eng. Chem. Res.* 54 (2015) 7226e7232.
- [184] L. Wang, L. Chang, B. Zhao, Z. Yuan, G. Shao, W. Zheng, Systematic investigation on morphologies, forming mechanism, photocatalytic and photoluminescent properties of ZnO nanostructures constructed in ionic liquids, *Inorg. Chem.* 47 (2008) 1443e1452.
- [185] G.P. Awasthi, S.P. Adhikari, S. Ko, H.J. Kim, C.H. Park, C.S. Kim, Facile synthesis of ZnO flowers modified graphene like MoS₂ sheets for enhanced visiblelight- driven photocatalytic activity and antibacterial properties, *J. Alloys Compd.* 682 (2016) 208e215.
- [186] S. Sharma, S.K. Mehta, S.K. Kansal, N doped ZnO/C-dots nanoflowers as visible light driven photocatalyst for the degradation of malachite green dye in aqueous phase, *J. Alloys Compd.* 699 (2017) 323e333.
- [187] K.-J. Kim, P.B. Kreider, C. Choi, C.-H. Chang, H.-G. Ahn, Visible-light sensitive Na-doped p-type flower-like ZnO photocatalysts synthesized via a continuous flow microreactor, *RSC Adv.* 3 (2013) 12702e12710.
- [188] A. Tabib, W. Bouslama, B. Sieber, A. Addad, H. Elhouichet, M. F_erid, R. Boukherroub, Structural and optical properties of Na doped ZnO nanocrystals: application to solar photocatalysis, *Appl. Surf. Sci.* 396 (2017) 1528e1538.
- [189] M. Yousefi, R. Azimirad, M. Amiri, A.Z. Moshfegh, Effect of annealing temperature on growth of Ce-ZnO nanocomposite thin films: X-ray photoelectron spectroscopy study, *Thin Solid Films* 520 (2011) 721e725.
- [190] M. Rezaei, A. Habibi-Yangjeh, Microwave-assisted preparation of Ce-doped ZnO nanostructures as an efficient photocatalyst, *Mater. Lett.* 110 (2013) 53e56.
- [191] Q. Zhang, J.-K. Liu, J.-D. Wang, H.-X. Luo, Y. Lu, X.-H. Yang, Atmospheric selfinduction synthesis and enhanced visible light photocatalytic performance of Fe₃ doped Ag-ZnO mesocrystals, *Ind. Eng. Chem. Res.* 53 (2014) 13236e13246.
- [192] R. He, R.K. Hocking, T. Tsuzuki, Co-doped ZnO nanopowders: location of cobalt and reduction in photocatalytic activity, *Mater. Chem. Phys.* 132 (2012) 1035e1040.
- [193] Q. Yin, R. Qiao, Z. Li, X.L. Zhang, L. Zhu, Hierarchical nanostructures of nickeldoped zinc oxide: morphology controlled synthesis and enhanced visible light photocatalytic activity, *J. Alloys Compd.* 618 (2015) 318e325.
- [194] R. Ullah, J. Dutta, Photocatalytic degradation of organic dyes with manganese-doped ZnO nanoparticles, *J. Hazard. Mater.* 156 (2008) 194e200.
- [195] C.-J. Chang, T.-L. Yang, Y.-C. Weng, Synthesis and characterization of Crdoped ZnO nanorod-array photocatalysts with improved activity, *J. Solid State Chem.* 214 (2014) 101e107.
- [196] R. Slama, F. Ghribi, A. Houas, C. Barthou, L. El Mir, Visible photocatalytic properties of vanadium doped zinc oxide aerogel nanopowder, *Thin Solid Films* 519 (2011) 5792e5795.
- [197] M. Fu, Y. Li, S. wu, P. Lu, J. Liu, F. Dong, Solgel preparation and enhanced photocatalytic performance of Cu-doped ZnO nanoparticles, *Appl. Surf. Sci.* 258 (2011) 1587e1591.
- [198] N. Clament Sagaya Selvam, J.J. Vijaya, L.J. Kennedy, Effects of morphology and Zr doping on structural, optical, and photocatalytic properties of ZnO nanostructures, *Ind. Eng. Chem. Res.* 51 (2012) 16333e16345.
- [199] M. Rezaei, A. Habibi-Yangjeh, Simple and large scale refluxing method for preparation of Ce-doped ZnO nanostructures as highly efficient photocatalyst, *Appl. Surf. Sci.* 265 (2013) 591e596.
- [200] N. Kannadasan, N. Shanmugam, S. Cholan, K. Sathishkumar, G. Viruthagiri, R. Poonguzhali, The effect of Ce⁴⁺ incorporation on structural, morphological and photocatalytic characters of ZnO nanoparticles, *Mater. Charact.* 97 (2014) 37e46.
- [201] M. Yousefi, M. Amiri, R. Azimirad, A.Z. Moshfegh, Enhanced photoelectrochemical activity of Ce doped ZnO nanocomposite thin films under visible light, *J. Electroanal. Chem.* 661 (2011) 106e112.

- [202] M. Yousefi, R. Azimirad, M. Amiri, A.Z. Moshfegh, Effect of annealing temperature on growth of Ce-ZnO nanocomposite thin films: X-ray photoelectron spectroscopy study, *Thin Solid Films* 520 (2011) 721e725.
- [203] M. Rezaei, A. Habibi-Yangjeh, Microwave-assisted preparation of Ce-doped ZnO nanostructures as an efficient photocatalyst, *Mater. Lett.* 110 (2013) 53e56.
- [204] S.R. Kadam, V.R. Mate, R.P. Panmand, L.K. Nikam, M.V. Kulkarni, R.S. Sonawane, B.B. Kale, A green process for efficient lignin (biomass) degradation and hydrogen production via water splitting using nanostructured C, N, S-doped ZnO under solar light, *RSC Adv.* 4 (2014) 60626e60635.
- [205] L.-C. Chen, Y.-J. Tu, Y.-S. Wang, R.-S. Kan, C.-M. Huang, Characterization and photoreactivity of N-, S-, and C-doped ZnO under UV and visible light illumination, *J. Photochem. Photobiol. A* 199 (2008) 170e178.
- [206] Z. Li, S. Sun, X. Xu, B. Zheng, A. Meng, Photocatalytic activity and DFT calculations on electronic structure of N-doped ZnO/Ag nanocomposites, *Catal. Commun.* 12 (2011) 890e894.
- [207] Z. Yu, L.-C. Yin, Y. Xie, G. Liu, X. Ma, H.-M. Cheng, Crystallinity-dependent substitutional nitrogen doping in ZnO and its improved visible light photocatalytic activity, *J. Colloid Interf. Sci.* 400 (2013) 18e23.
- [208] C. Di Valentin, G. Pacchioni, Spectroscopic properties of doped and defective semiconducting oxides from hybrid density functional calculations, *Acc. Chem. Res.* 47 (2014) 3233e3241.
- [209] F. Gallino, C. Di Valentin, G. Pacchioni, M. Chiesa, E. Giamello, Nitrogen impurity states in polycrystalline ZnO. A combined EPR and theoretical study, *J. Mater. Chem. C* 20 (2010) 689e697.
- [210] S. Liu, C. Li, J. Yu, Q. Xiang, Improved visible-light photocatalytic activity of porous carbon self-doped ZnO nanosheet-assembled flowers, *CrystEngComm* 13 (2011) 2533e2541.
- [211] S. Cho, J.-W. Jang, J.S. Lee, K.-H. Lee, Carbon-doped ZnO nanostructures synthesized using vitamin C for visible light photocatalysis, *CrystEngComm* 12 (2010) 3929e3935.
- [212] W. Yu, J. Zhang, T. Peng, New insight into the enhanced photocatalytic activity of N-, C- and S-doped ZnO photocatalysts, *Appl. Catal. B Environ.* 181 (2016) 220e227.
- [213] S. Kuriakose, B. Satpati, S. Mohapatra, Enhanced photocatalytic activity of Co doped ZnO nanodisks and nanorods prepared by a facile wet chemical method, *Phys. Chem. Chem. Phys.* 16 (2014) 12741e12749.
- [214] A. Hui, J. Ma, J. Liu, Y. Bao, J. Zhang, Morphological evolution of Fe doped sea urchin-shaped ZnO nanoparticles with enhanced photocatalytic activity, *J. Alloys Compd.* 696 (2017) 639e647.
- [215] L.C.-K. Liao, J.-S. Huang, Energy-level variations of Cu-doped ZnO fabricated through sol-gel processing, *J. Alloys Compd.* 702 (2017) 153e160.
- [216] Q. Deng, H. Tang, G. Liu, X. Song, G. Xu, Q. Li, D.H.L. Ng, G. Wang, The fabrication and photocatalytic performances of flower-like Ag nanoparticles/ZnO nanosheets-assembled microspheres, *Appl. Surf. Sci.* 331 (2015) 50e57.
- [217] Z. Xuming, C. Yu Lim, L. Ru-Shi, and T. Din Ping, *Rep. Prog. Phys.* 76, 046401 (2013).
- [218] Rezaei M, Habibi-Yangjeh A. Simple and large scale refluxing method for preparation of Ce-doped ZnO nanostructures as highly efficient photocatalyst. *Appl Surf Sci* 2013; 265:591–6. <http://dx.doi.org/10.1016/j.apsusc.2012.11.053>.
- [219] Y. Wang, H.-B. Fang, Y.-Z. Zheng, R. Ye, X. Tao, J.-F. Chen, Controllable assembly of well-defined monodisperse Au nanoparticles on hierarchical ZnO microspheres for enhanced visible-light-driven photocatalytic and antibacterial activity, *Nanoscale* 7 (2015) 19118e19128.
- [220] Bora, T., Myint, M. T. Z., Al-Harhi, S. H. & Dutta, J. Role of surface defects on visible light enabled plasmonic photocatalysis in Au-ZnO nanocatalysts, *RSC Adv.* 5, 96670 (2015).
- [221] Zhang, P. et al. Core/shell nanofibers of TiO₂ @carbon embedded by Ag nanoparticles with enhanced visible photocatalytic activity. *J. Mater. Chem.* 21, 17746- 17753 (2011).
- [222] Naya, S.-I., Inoue, A. & Tada, H. Self-assembled heterosupramolecular visible light photocatalyst consisting of gold nanoparticle-loaded titanium (IV) dioxide and surfactant. *J. Am. Chem. Soc.* 132, 6292-6293 (2008).
- [223] Saoud, K. et al. Synthesis of supported silver nano-spheres on zinc oxide nanorods for visible light photocatalytic applications. *Mater. Res. Bull.* 63, 134- 140 (2015).
- [224] Hao, Q. et al. Aluminium plasmonic photocatalysis. *Sci. Rep.* 5, 15288 (2015)
- [225] Y. Tian, and T. Tatsuma, *J. Am. Chem. Soc.* 127, 7632 (2005).

- [226] S. Sarina, E. R. Waclawik, and H. Zhu, *Green Chem.* 15, 1814 (2013).
- [227] Chen, X., Zhu, H.-Y., Zhao, J.-C., Zheng, Z.F., & Gao, X.-P. Visible-light-driven oxidation of organic contaminants in air with gold nanoparticle catalysts on oxide supports. *Angew. Chem. Int. Ed.* 120, 5433-5436 (2008).
- [228] C. Tian, Q. Zhang, B. Jiang, G. Tian, H. Fu, Glucose-mediated solution-solid route for easy synthesis of Ag/ZnO particles with superior photocatalytic activity and photostability, *J. Alloys Compd.* 509 (2011) 6935e6941.
- [229] C. Gu, C. Cheng, H. Huang, T. Wong, N. Wang, T.-Y. Zhang, Growth and photocatalytic activity of dendrite-like ZnO@Ag heterostructure nanocrystals, *Cryst. Growth Des.* 9 (2009) 3278e3285.
- [230] C. Pacholski, A. Kornowski, H. Weller, Site-specific photodeposition of silver on ZnO nanorods, *Angew. Chem. Int. Ed.* 43 (2004) 4774e4777.
- [231] J. Liqiang, W. Dejun, W. Baiqi, L. Shudan, X. Baifu, F. Honggang, S. Jiazong, Effects of noble metal modification on surface oxygen composition, charge separation and photocatalytic activity of ZnO nanoparticles, *J. Mol. Catal. A Chem.* 244 (2006) 193e200.
- [232] Reza M. Coupled semiconductor metal oxide nanocomposites: types, synthesis conditions and properties. *Adv. Compos. Mater. Med. Nanotechnol. InTech*; 2011. <http://dx.doi.org/10.5772/1435>.
- [233] Chiang Y-J, Lin C-C. Photocatalytic decolorization of methylene blue in aqueous solutions using coupled ZnO/SnO₂ photocatalysts. *Powder. Technol* 2013;246:137–43. <http://dx.doi.org/10.1016/j.powtec.2013.04.033>.
- [234] Yang G, Yan Z, Xiao T. Preparation and characterization of SnO₂/ZnO/TiO₂ composite semiconductor with enhanced photocatalytic activity. *Appl Surf Sci* 2012;258:8704–12. <http://dx.doi.org/10.1016/j.apsusc.2012.05.078>.
- [235] Wang H, Baek S, Lee J, Lim S. High photocatalytic activity of silver-loaded ZnO/SnO₂ coupled catalysts. *Chem Eng J* 2009;146:355–61. <http://dx.doi.org/10.1016/j.cej.2008.06.016>.
- [236] Zhang M, An T, Hu X, Wang C, Sheng G, Fu J. Preparation and photocatalytic properties of a nanometer ZnO–SnO₂ coupled oxide. *Appl Catal A Gen* 2004;260:215–22. <http://dx.doi.org/10.1016/j.apcata.2003.10.025>.
- [238] Moradi S, Aberoomand-Azar P, Raeis-Farshid S, Abedini-Khorrami S, Givianrad MH. The effect of different molar ratios of ZnO on characterization and photocatalytic activity of TiO₂/ZnO nanocomposite. *J Saudi Chem Soc* 2016;20:373–8. <http://dx.doi.org/10.1016/j.jscs.2012.08.002>.
- [239] Li C, Liu Q, Shu S, Xie Y, Zhao Y, Chen B, et al. Preparation and characterization of regenerated cellulose/TiO₂/ZnO nanocomposites and its photocatalytic activity. *Mater Lett* 2014;117. <http://dx.doi.org/10.1016/j.matlet.2013.12.009>.
- [240] Zhu H, Jiang R, Fu Y, Guan Y, Yao J, Xiao L, et al. Effective photocatalytic decolorization of methyl orange utilizing TiO₂/ZnO/chitosan nanocomposite films under simulated solar irradiation. *Desalination* 2012;286:41–8. <http://dx.doi.org/10.1016/j.desal.2011.10.036>.
- [241] Liu Y, Zhu G, Chen J, Xu H, Shen X, Yuan A. Co₃O₄/ZnO nanocomposites for gassensing applications. *Appl Surf Sci* 2013;265:379–84. <http://dx.doi.org/10.1016/j.apsusc.2012.11.016>.
- [242] B. Li, H. Cao, ZnO@graphene composite with enhanced performance for the removal of dye from water, *J. Mater. Chem.* 21 (2011) 3346e3349.
- [243] X. Liu, L. Pan, T. Lv, T. Lu, G. Zhu, Z. Sun, C. Sun, Microwave-assisted synthesis of ZnO/graphene composite for photocatalytic reduction of Cr(VI), *Catal. Sci. Technol.* 1 (2011) 1189e1193.
- [244] X. Bai, L. Wang, Y. Zhu, Visible photocatalytic activity enhancement of ZnWO₄ by graphene hybridization, *ACS Catal.* 2 (2012) 2769e2778.
- [245] S. Cao, J. Yu, Carbon-based H₂-production photocatalytic materials, *J. Photochem. Photobiol. C* 27 (2016) 72e99.
- [246] K.M. Cho, K.H. Kim, H.O. Choi, H.-T. Jung, A highly photoactive, visible-light-driven graphene/2D mesoporous TiO₂ photocatalyst, *Green Chem.* 17 (2015) 3972e3978.
- [247] Liu Y, Zhu G, Chen J, Xu H, Shen X, Yuan A. Co₃O₄/ZnO nanocomposites for gassensing applications. *Appl Surf Sci* 2013;265:379–84. <http://dx.doi.org/10.1016/j.apsusc.2012.11.016>.

- [248] Zhang Y, Mu J. Controllable synthesis of flower- and rod-like ZnO nanostructures by simply tuning the ratio of sodium hydroxide to zinc acetate. *Nanotechnology* 2007;18:75606. <http://dx.doi.org/10.1088/0957-4484/18/7/075606>.
- [249] Akir S, Barras A, Coffinier Y, Bououdina M, Boukherroub R, Omrani AD. Ecofriendly synthesis of ZnO nanoparticles with different morphologies and their visible light photocatalytic performance for the degradation of Rhodamine B. *Ceram Int* 2016;42:10259–65. <http://dx.doi.org/10.1016/j.ceramint.2016.03.153>.
- [250] Becker J, Raghupathi KR, St. Pierre J, Zhao D, Koodali RT. Tuning of the crystallite and particle sizes of ZnO nanocrystalline materials in solvothermal synthesis and their photocatalytic activity for dye degradation. *J Phys Chem C* 2011;115:13844–50. <http://dx.doi.org/10.1021/jp2038653>.
- [251] Hong R, Pan T, Qian J, Li H. Synthesis and surface modification of ZnO nanoparticles. *Chem Eng J* 2006;119:71–81. <http://dx.doi.org/10.1016/j.cej.2006.03.003>.
- [252] Farzi GA, Tayebie R, Naghibinasab S. Surface modification of ZnO nano-particles with trimethoxyvinyl silane and oleic acid and studying their dispersion in organic media. *Int J Nano Dimens* 2015;6:67–75. <http://dx.doi.org/10.7508/IJND.2015.06.009>.
- [253] <http://helpthe7seas.blogspot.com/2017/01/in-2050-there-will-be-more-plastic-then.html>
- [254] <https://www.sintef.no/imagevault/publishedmedia/gmhyws7xvz9vi6vuqy4j/bilde.jpg>
- [255] <https://wallaceterrycjr.files.wordpress.com/2014/12/energybands.jpg>
- [256] <https://umdrighnow.umd.edu/sites/umdrighnow.umd.edu/files/solarwatersplitting.jpg>
- [257] http://pubs.rsc.org/services/images/RSCpubs.ePlatform.Service.FreeContent.ImageService.svc/ImageService/Articleimage/2014/CP/c3cp55317e/c3cp55317e-f1_hi-res.gif
- [258] https://pubs.rsc.org/services/images/RSCpubs.ePlatform.Service.FreeContent.ImageService.svc/ImageService/Articleimage/2014/CS/c3cs60262a/c3cs60262a-f1_hi-res.gif
- C. Ong, L. Yong Ng and A. Mohammad, A review of ZnO nanoparticles as solar photocatalysts: Synthesis, mechanisms and applications, *Renewable and Sustainable Energy Reviews*, 81 (2018) 536–551.
- [260] Baruah, S., Mahmood, M. A., Myint, M. T. Z., Bora, T., & Dutta, J. (2010). Enhanced visible light photocatalysis through fast crystallization of zinc oxide nanorods. *Beilstein Journal of Nanotechnology*, 1, 14–20. <http://doi.org/10.3762/bjnano.1.3>.
- [261] M.A. Mahmood, T. Bora and J. Dutta, *Int. J. Environmental Technology and Management*, Vol. 16, Nos. 1/2, 2013.
- [262] T. Bora et al. Defect engineered visible light active ZnO nanorods for photocatalytic treatment of water, *Catalysis Today*, 2016.
- [263] https://www.researchgate.net/profile/Yang_Bingjun/publication/279736583/figure/fig1/AS:284636149239824@1444873954888/Schematic-band-diagram-and-transfer-process-of-GQDs-coated-ZNRA-CB-and-VB-represent-the.png.